Synthesis, structural characterization and antibacterial activity evaluation of novel quinolone-1,2,3-triazole-benzimidazole hybrids

Khadija El Gadali, Meriem Rafya, Az-Eddine El Mansouri, Mohamed Maatallah, Arie Van-Derlee, Ahmad Mehdi, Abdelaaziz Ouahrouch, Fatiha Benkhalti, Yogesh Sanghvi, Moha Taourirte, et al.

Synthesis, structural characterization and antibacterial activity evaluation of novel quinolone-1,2,3-triazole-benzimidazole hybrids

Khadija El Gadali,[a,b] Meriem Rafya,[a] Az-eddine El Mansouri,[c] Mohamed Maatallah,[b] Arie Vanderlee,[d] Ahmad Mehdi,[e] Abdelaaziz Ouahrouch,[a] Fatiha Benkhalti,[a] Yogesh S. Sanghvi,[f] Moha Taourirte,*[a] Hassan B. Lazrek.*[b]

[a] *Laboratoire de Recherche en développement durable et santé, Faculty of Sciences and Technology Gueliz (FSTG), BP549, Marrakech 40000, Morocco*

[b] *Laboratory of molecular Chemistry, Department of Chemistry, Faculty of Sciences Semlalia, Marrakech 40000, Morocco*

[c] *University of the free state Faculty of natural and agricultural sciences Chemistry department 205 Nelson Mandela, Bloemfontein, 9301, Republic of South Africa*

[d] *Institut Européen des Membranes, IEM, UMR 5635, Univ. Montpellier, CNRS, ENSCM, 34095 Montpellier, France*

[e] *ICGM, UMR5253 1919, Route de Mende 34293 Montpellier cedex 5*

[f] *Rasayan Inc. 2802 Crystal Ridge Road, Encinitas, CA 92024-6615, USA*

*Corresponding authors: hblazrek50@gmail.com, m.taourirte@uca.ma

Abstract

In this investigation, a series of 2-quinolone-benzimidazole hybrids linked by a 1,2,3-triazole moiety were prepared using copper-catalyzed Huisgen 1,3-dipolar cycloaddition and condensation reaction. The newly synthesized compounds were characterized by ^{1}H NMR, ^{13}C NMR, single crystal XRD and HRMS analysis. The density functional theory (DFT) calculations were performed using B3LYP/6-31+G(d,p) basis level set for the optimization of molecular geometries of compounds **7a**, **7c**, **7f** and **7l**. The conformational analysis predicted the existence of two main conformations: a closed and an open conformation. *In vitro* antibacterial activity was assessed against Gram-positive bacterium *Staphylococcus aureus (S. aureus)* and Gram-negative bacterium *Escherichia coli (E. coli)*. The bioassays revealed that compounds **7a**, **7c**, **7f** and **7l** inhibited the growth of *E. coli* at a concentration of 0.14 µmol/mL, which was nearly 2-fold stronger than the control drug ampicillin (0.26 µmol/mL). Besides, compounds **7f** and **7l** exhibited the most promising activity against *S. aureus* with MIC and MBC values of 0.07 µmol/mL for **7f** and 0.14 µmol/mL for **7l** compared to 0.27 µmol/mL for ampicillin. These results were supported by the chemical reactivity parameters and electrostatic surface potential (MEP) obtained using theoretical calculations. Molecular docking study of the most active compounds using DNA gyrase A and DNA gyrase B proteins of *S. aureus* also confirmed the experimental findings.

Keywords: 2-quinolone, benzimidazole, 1,2,3-triazole, antibacterial activity, molecular docking, DFT studies.

Graphical abstract

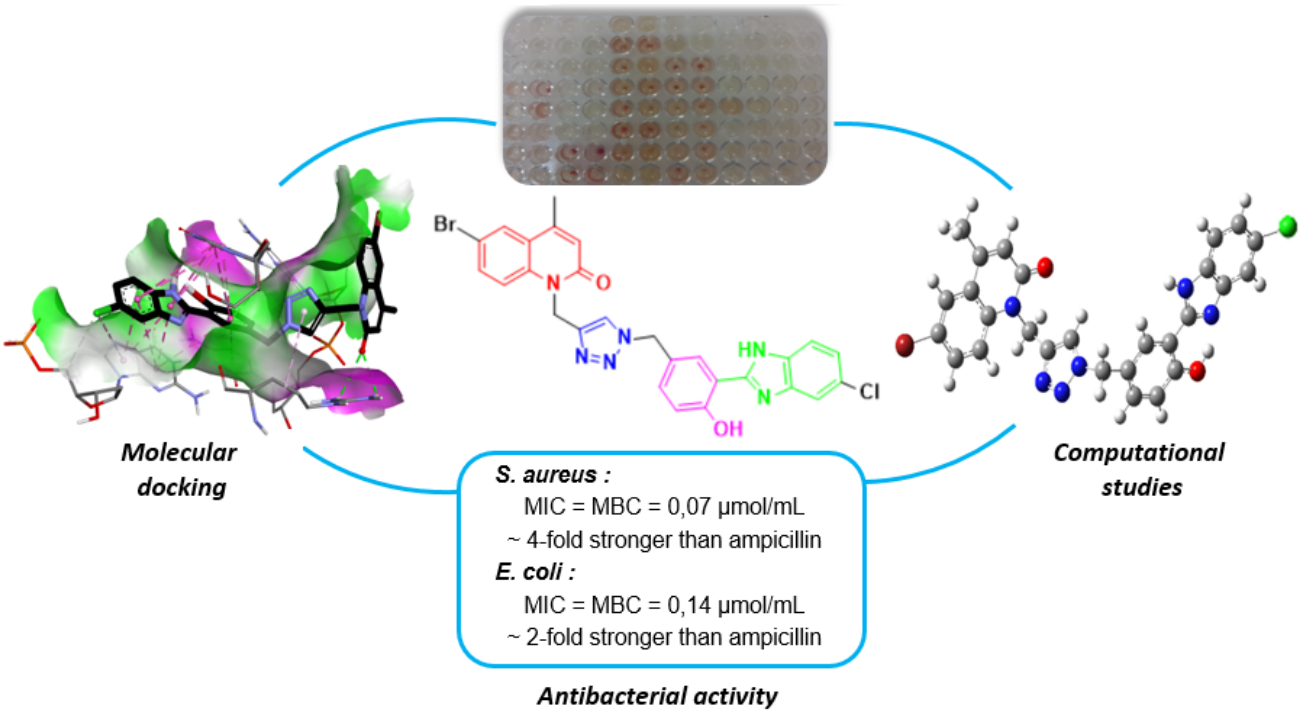

1. Introduction

According to the WHO, antimicrobial resistance (AMR) is a growing threat to human health globally. This phenomenon occurs when germs like bacteria and fungi develop mutations that make antibiotics ineffective [1]. Among these germs is *S. aureus*, which has the ability to develop resistance to many antimicrobial agents. It can induce various clinical diseases, including mild skin and soft tissue infections, bacteremia, infective endocarditis and osteomyelitis [2]. Additionally, *S. aureus* is the primary causative strain of severe secondary bacterial pneumonia following influenza A virus (IAV) infection, which results in significant morbidity and mortality [3]. More importantly, it has been found that *S. aureus* triggers respiratory complications in patients hospitalized with COVID-19 and is associated with high case fatality rate [4]. Based on these facts, there is a continuous necessity for the search of new effective antimicrobial drugs to overcome bacterial resistance. The 2-quinolone nucleus is one of the most useful frameworks in the synthesis and development of impending antibiotics. 2-Quinolones and their analogues are important nitrogen-containing heterocycles, widely present in nature as alkaloids (such as Viridicatol or Viridicatin (Fig. 1)) [5–8] and possess an extensive spectrum of biological properties among which is the antimicrobial [9,10]. Many of the quinolone-based scaffolds with antibacterial activity, were found to act mainly by inhibiting the activity of bacteria type II topoisomerase (DNA gyrase) or type IV topoisomerase [11]. Both enzymes are important for bacterial cell survival and are involved in the control of topological transitions of DNA. Consequently, DNA gyrase and topoisomerase IV represent attractive targets in the design of antibacterial therapeutics [12,13].

Molecular hybridization emerges as one of the best used strategies in the construction of new pharmaceutical compounds [14–16]. This is based on the formation of potentially active molecules by joining pharmacophore moieties of different bioactive substances [17]. Therefore, the combination of 2-quinolone and other heterocyclic compounds such as 1,2,3-triazole and benzimidazole may lead to a much more potent antibacterial agent. 1,2,3-Triazoles are quite attractive for medicinal chemistry applications and have become increasingly employed as linker units owing to their high biocompatibility and stability under various chemical conditions [18]. They show very long range of biological activities such as antimicrobial (Fig. 1) [19,20], antiviral [21] and anticancer [22]. On the other hand, benzimidazoles are known to exhibit diverse pharmacological activities and are present in numerous drugs, including Thiabendazole (antihelmintic and antimicrobial drug) [23,24], Bendamustine (anticancer drug) [25], Domperidone (antiemitic drug) [26], Pimozide (antipsychotic drug) [27], etc. Specifically, benzimidazolyl-phenol is considered a privileged structure due to its chelating characteristics and fluorescence properties [28,29]. Moreover, many benzimidazolyl-phenol

derivatives and some of their metal complexes were reported to have significant antimicrobial effect on Gram-negative bacteria and Gram-positive ones [30,31].

In light of the aforementioned data, we report herein the synthesis of novel hybrid molecules that covalently connect 4-methyl-(1*H*)-quinolin-2-one and benzimidazole *via* a triazole ring. Although much work has been done to assess the biological potency of 4-methyl substituted 2-quinolone [32–34], its 6-halogeneted derivatives are still insufficiently studied. Hence, we elected to use 6-bromo/fluoro-4-methyl-(1*H*)-quinolin-2-one as a starting point for producing new potential antibiotics. All synthesized compounds were screened against *E. coli* and *S. aureus* using broth microdilution MIC method. DFT calculations were used to optimize the molecular geometries and define reactivity indexes. Molecular docking was also conducted to understand the binding mechanism of compounds that best inhibited the growth of *S. aureus*. Further, single crystal X-ray study of compounds **6b** and **7a** has been reported.

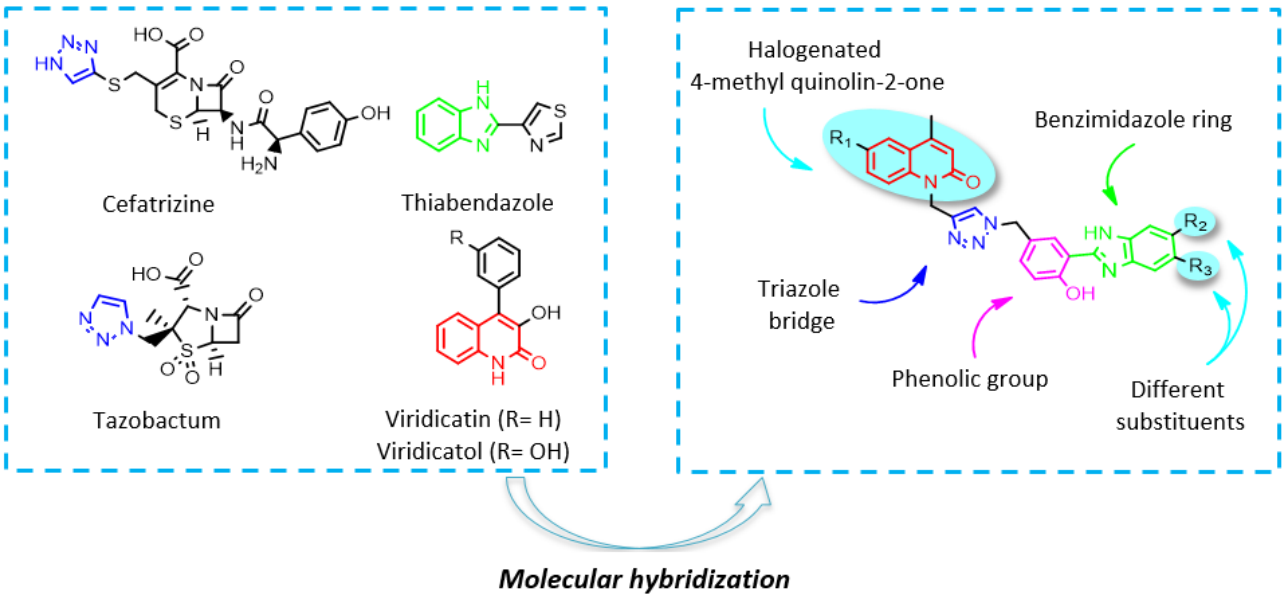

Fig. 1. Examples of antimicrobial agents and design strategy of target structures.

2. Experimental

2.1. Synthesis and characterization

Melting points were measured using a Büchi B-545 digital capillary melting point apparatus and are uncorrected. NMR spectra were recorded at 300 MHz (^{1}H, ^{13}C) Bruker in (DMSO-d_6, $CDCl_3$) using TMS as an internal reference. All chemical shifts (δ) are expressed in parts per million and coupling constant (J) are given in Hertz and multiplicities of the signals are indicated by the following abbreviations: s, singlet; d, doublet; t, triplet; q, quadruplet; dd, doublet of doublets; td, triplet of

doublets and m, multiplet. LC-UV-MS was performed using a Dionex Ultimate 3000 LC system equipped with DAD and Thermo TSQ Endura mass spectrometer. HRMS (ESI) was determined by using micrOTOF-Q. Precoated Merck Silica Gel 60F-254 plates were used for thin layer chromatography (TLC) and the spots were detected under UV light (254 nm). Column chromatography (CLC) was performed using silica gel (0.063-0.2 mm) Fluka. All reagents used were purchased from Fluka/Sigma-Aldrich.

General procedure for the synthesis of alkynes (2 and 3).

A mixture of quinolone **1a** or **1b** (1 mmol), K_2CO_3 (1 mmol) and propargyl bromide (1.5 mmol) in anhydrous acetonitrile (5 mL) was stirred at 90°C during 5h. After removal of the solvent under reduced pressure the residue obtained was purified on a silica gel column eluted with (hexane /EtOAc 95:5) then (CH_2Cl_2).

6-Bromo-4-methyl-1-(prop-2-yn-1-yl) quinolin-2(1*H*)-one (2a)

Yield 60%, white solid, Rf: 0.2 (CH_2Cl_2), Mp (°C) 200-202, ^{1}H NMR (300 MHz, $CDCl_3$) δ 7.74 (d, 1H, J = 2.3 Hz, Ar-H), 7.60 (dd, 1H, J = 9.0, 2.3 Hz, Ar-H), 7.33 (d, 1H, J = 9.0 Hz, Ar-H), 6.53 (s, 1H, –C=CH), 4.99 (d, 2H, J = 2.5 Hz, CH_2), 2.36 (s, 3H, CH_3), 2.17 (t, 1H, J = 2.5 Hz, –C≡CH). ^{13}C NMR (75 MHz, $CDCl_3$) δ 160.63, 146.17, 137.37, 133.28, 127.95, 121.81, 116.65, 115.50, 77.76, 72.70, 31.42, 19.00. LC-MS (ESI) m/z 276.00 $[M+H]^+$; HRMS (ESI) calculated for $C_{13}H_{10}BrNO$ $[M+H]^+$ 276.0019, found 276.0027.

6-Fluoro-4-methyl-1-(prop-2-yn-1-yl) quinolin-2(1*H*)-one (2b)

Yield 66%, colorless crystals, Rf: 0.16 (CH_2Cl_2), Mp (°C) 161-163, ^{1}H NMR (300 MHz, $CDCl_3$) δ 7.41 (dd, 1H, J = 9.0, 4.5 Hz, Ar-H), 7.36 – 7.18 (m, 2H, Ar-H), 6.53 (s, 1H, –C=CH), 4.99 (d, 2H, J = 2.5 Hz, CH_2), 2.33 (s, 3H, CH_3), 2.18 (t, 1H, J = 2.4 Hz, –C≡CH). ^{13}C NMR (75 MHz, $CDCl_3$) δ 160.6, 158.00 (d, J_{C-F} = 242.4 Hz), 146.30 (d, J_{C-F} = 3.3 Hz), 134.87, 122.74 (d, J_{C-F} = 8.0 Hz), 121.82, 118.11 (d, J_{C-F} = 23.7 Hz), 116.49 (d, J_{C-F}= 8.0 Hz), 110.86 (d, J_{C-F} = 23.3 Hz), 77.96, 72.59, 31.51, 19.00. LC-MS (ESI) m/z 216.08 $[M+H]^+$; HRMS (ESI) calculated for $C_{13}H_{10}FNO$ $[M+H]^+$ 216.0819, found 216.0825.

6-Bromo-4-methyl-2-(prop-2-yn-1-yloxy)quinoline (3a)

Yield 17%, white solid, Rf: 0.54 (hexane/ethyl acetate, 9.5/0.5), Mp (°C) 97-99, ^{1}H NMR (300 MHz, $CDCl_3$) δ 7.89 (d, 1H, J = 1.6 Hz, Ar-H), 7.66 – 7.53 (m, 2H, Ar-H), 6.72 (s, 1H, –C=CH), 5.02 (d, 2H, J = 2.4 Hz, CH_2), 2.49 (s, 2H, CH_3), 2.42 (t, 1H, J = 2.4 Hz, –C≡CH). ^{13}C NMR δ (75 MHz, $CDCl_3$) δ 159.64, 145.34, 143.86, 131.52, 128.55, 125.93, 125.14, 116.60, 112.52, 78.11, 73.35, 52.29,

17.61. LC-MS (ESI) m/z 276.00 $[M+H]^+$; HRMS (ESI) calculated for $C_{13}H_{10}BrNO$ $[M+H]^+$ 276.0019, found 276.0018.

6-Fluoro-4-methyl-2-(prop-2-yn-1-yloxy)quinoline (3b)

Yield 19%, white solid, Rf: 0.52 (hexane/ethyl acetate, 9.5/0.5), Mp (°C) 82-84, ^{1}H NMR (300 MHz, $CDCl_3$) δ 7.73 (dd, 1H, J = 9.1, 5.4 Hz, Ar-H), 7.38 (dd, 1H, J = 9.8, 2.9 Hz, Ar-H), 7.28 (td, 1H, J = 8.6, 2.9 Hz, Ar-H), 6.73 (s, 1H, –C=CH), 5.02 (d, 2H, J = 2.4 Hz, CH_2), 2.48 (s, 3H, CH_3), 2.41 (t, 1H, J = 2.4 Hz, –C≡CH). ^{13}C NMR (75 MHz, $CDCl_3$) δ 160.05, 159.23 (d, J_{C-F} = 243.9 Hz), 157.63, 146.57 (d, J_{C-F} = 4.9 Hz), 142.96, 129.85 (d, J_{C-F} = 8.8 Hz), 126.17 (d, J_{C-F} = 8.9 Hz), 118.64 (d, J_{C-F} = 24.8 Hz), 113.42, 107.76 (d, J_{C-F}= 22.4 Hz), 79.30, 74.28, 53.20, 18.69. LC-MS (ESI) m/z 216.08 $[M+H]^+$; HRMS (ESI) calculated for $C_{13}H_{10}FNO$ $[M+H]^+$ 216.0819, found 216.0821.

General procedure for the synthesis of azide (5)

According to a previously reported method [35], salicylaldehyde (48 mmol) was added to a mixture of formaldehyde (37% in H_2O, 3.6 mL) and hydrochloric acid (37%, 48 mL) and the reaction stirred overnight at room temperature. The solid that formed was filtered and recrystallized from hot hexane to give **4** as white crystalline solid. Subsequently, 5-chloromethyl salicylaldehyde **4** (11 mmol) was dissolved in water-acetone (1:1) and successively was added to a solution of sodium azide (5eq, 10 ml) at 0°C. The mixture was stirred for 12h at room temperature and extracted with ethyl acetate (3 × 15 mL). Lastly, the extract was evaporated under reduced pressure, and the residue was purified by flash chromatography column (hexane /EtOAc 98:2).

5-(Azidomethyl)-2-hydroxybenzaldehyde (5)

Yield 92%, white crystals, Rf: 0.17 (hexane/ethyl acetate, 9.9/0.1), ^{1}H NMR (300 MHz, $CDCl_3$) δ 11.06 (s, 1H, OH), 9.92 (s, 1H, CHO), 7.54 (d, J = 1.8 Hz, 1H, Ar-H), 7.50 (dd, J = 8.7, 1.7 Hz, 1H, Ar-H), 7.04 (d, J = 8.5 Hz, 1H Ar-H), 4.36 (s, 2H, CH_2). ^{13}C NMR (75 MHz, $CDCl_3$) δ 196.24, 161.58, 136.88, 133.18, 127.12, 120.43, 118.39, 53.78.

General procedure for the synthesis of triazole derivatives (6a-b)

A mixture of N-propargylquinolone **2a,b** (2 mmol) in 5 ml of dimethyl formamide (DMF), Et_3N (2 mmol), CuI (0.2 mmol) and azide **5** (2,4 mmol) was heated at 95°C for 1h. After removal of the solvent under reduced pressure, the residue was purified by flash chromatography eluting with (CH_2Cl_2/MeOH 99:1).

5-((4-((6-Bromo-4-methyl-2-oxoquinolin-1(2*H*)-yl)methyl)-1*H*-1,2,3-triazol-1-yl)methyl)-2-hydroxybenzaldehyde 6a

Yield 80%, white solid, Rf: 0.34 (CH_2Cl_2/CH_3OH: 9.8/0.2), Mp (°C) 220-222, ^{1}H NMR (300 MHz, $CDCl_3$) δ 10.96 (s, 1H, OH), 9.76 (s, 1H, CHO), 7.75 (d, J = 9.1 Hz, 1H, Ar-H), 7.69 (d, J = 2.2 Hz, 1H, Ar-H), 7.56 (dd, J = 9.0, 2.2 Hz, 1H, Ar-H), 7.53 (s, 1H, triazole-CH), 7.40 (d, J = 2.2 Hz, 1H, Ar-H), 7.36 (dd, J = 8.6, 2.3 Hz, 1H, Ar-H), 6.89 (d, J = 8.5 Hz, 1H, Ar-H), 6.51 (s, 1H, –C=CH), 5.42 (s, 2H, CH_2), 5.34 (s, 2H, CH_2), 2.35 (s, 3H, CH_3). ^{13}C NMR (75 MHz, $CDCl_3$) δ 196.05, 161.88, 161.46, 146.32, 144.05, 137.87, 136.77, 133.51, 133.43, 127.73, 125.92, 123.32, 123.10, 121.66, 120.50, 118.72, 117.19, 115.47, 53.20, 38.06, 19.03. LC-MS (ESI) m/z 453.05 $[M+H]^+$; HRMS (ESI) calculated for $C_{21}H_{17}BrN_4O_3$ $[M+H]^+$453.0557, found 453.0553.

5-((4-((6-Fluoro-4-methyl-2-oxoquinolin-1(2*H*)-yl)methyl)-1*H*-1,2,3-triazol-1-yl)methyl)-2-hydroxybenzaldehyde 6b

Yield 93%, colorless crystals, Rf: 0.27 (CH_2Cl_2/CH_3OH: 9.8/0.2), Mp (°C) 210-212, ^{1}H NMR (300 MHz, $CDCl_3$) δ 11.04 (s, 1H, OH), 9.83 (s, 1H, CHO), 7.92 (dd, 1H, J = 9.04.6 Hz, Ar-H), 7.62 (s, 1H, triazole-CH), 7.48 (d, J = 2.3 Hz, 1H, Ar-H), 7.43 (dd, J = 8.6, 2.3 Hz, 1H, Ar-H), 7.37 – 7.23 (m, 2H, Ar-H), 6.97 (d, 1H, J = 8.6 Hz, Ar-H), 6.61 (s, 1H, –C=CH), 5.51 (s, 2H, CH_2), 5.42 (s, 2H, CH_2), 2.41 (s, 3H, CH_3). ^{13}C NMR (75 MHz, $CDCl_3$) δ 196.01, 161.88, 161.47, 157.99 (d, J_{C-F} = 242.5 Hz), 146.43 (d, J_{C-F} = 3.1 Hz), 144.21, 136.74, 135.44, 133.41, 125.96, 123.35, 122.56 (d, J_{C-F} = 7.8 Hz), 121.75, 120.52, 118.70, 118.40 (d, J_{C-F} = 23.6 Hz), 117.10 (d, J_{C-F} = 8.1 Hz), 110.60 (d, J_{C-F} = 23.2 Hz), 53.18, 38.21, 19.02. LC-MS (ESI) m/z 393.14 $[M+H]^+$; HRMS (ESI) calculated for $C_{21}H_{17}FN_4O_3$ $[M+H]^+$ 393.1357, found 393.1366.

General procedure for the formation of compounds (7a-n)

Compounds **7a-n** were synthesized following a reported method with modification [36]. Briefly, a mixture of compound **6** (0.2 mmol), and 2 equivalents of sodium hydrogen sulfite were dissolved in water/ethanol (1:9) and stirred for 20 min at 40°C. Then 1 equivalent of the appropriate o-phenylenediamine was added to the mixture. The reaction mixture was allowed to stir at 40°C for 3 h. After completion of the reaction (monitored by TLC), the precipitate was filtered and purified by flash chromatography eluting with (CH_2Cl_2/MeOH 99:1).

1-((1-(3-(1*H*-benzo[d]imidazol-2-yl)-4-hydroxybenzyl)-1*H*-1,2,3-triazol-4-yl)methyl)-6-bromo-4-methylquinolin-2(1*H*)-one (7a)

Yield 46%, white solid, Rf: 0.24 (CH_2Cl_2/CH_3OH: 9.85/0.15), Mp (°C) 265-268, UV (CH_2Cl_2/CH_3OH: 1/1) λmax = 236, 333 nm, ^{1}H NMR (300 MHz, DMSO-d_6) δ 13.17 (s, 2H, OH+NH), 8.04 (s, 1H, Ar-H), 7.99 (s, 1H, Ar-H), 7.82 (s, 1H, Ar-H), 7.66 (d, J = 8.5 Hz, 2H, Ar-H), 7.61 (s, 1H, triazole-CH), 7.31 (d, J = 8.3 Hz, 2H, Ar-H), 7.25 (brs, 2H, Ar-H), 6.98 (d, J = 8.1 Hz, 1H, –C=CH),

6.56 (s, 1H, –C=CH), 5.47 (s, 2H, CH_2), 5.43 (s, 2H, CH_2), 2.36 (s, 3H, CH_3). ^{13}C NMR (75 MHz, $CDCl_3$) δ 160.83, 158.38, 151.61, 146.96, 143.54, 141.38, 138.32, 133.81, 133.54, 132.42, 128.17, 127.16, 126.99, 123.82, 123.22, 123.00, 121.80, 118.55, 118.06, 114.86, 113.38, 112.19, 53.16, 37.76, 18.96. LC-MS (ESI) m/z 541.10 $[M+H]^+$; HRMS (ESI) calculated for $C_{27}H_{21}BrN_6O_2$ $[M+H]^+$ 541.0982, found 541.0974.

6-Bromo-1-((1-(4-hydroxy-3-(5-methyl-1*H*-benzo[d]imidazol-2-yl)benzyl)-1*H*-1,2,3-triazol-4-yl)methyl)-4-methylquinolin-2(1*H*)-one (7b)

Yield 56%, white solid, Rf: 0.24 (CH_2Cl_2/CH_3OH: 9.85/0.15), Mp (°C) 220-224, UV (CH_2Cl_2/CH_3OH: 1/1) λmax = 236, 324 nm, ^{1}H NMR (300 MHz, DMSO-d_6) δ 13.23 (s, 1H, OH), 13.07 (s, 1H, NH), 8.04 (d, J = 1.9 Hz, 1H, Ar-H), 8.01 (s, 1H, Ar-H), 7.87 (s, 1H, Ar-H), 7.67 (dd, J = 22.0, 9.1 Hz, 2H, Ar-H), 7.60 – 7.36 (m, 2H, Ar-H), 7.33 (dd, J = 8.5, 2.0 Hz, 1H, Ar-H), 7.09 (d, J = 5.5 Hz, 1H, Ar-H), 7.00 (d, J = 8.4 Hz, 1H, Ar-H), 6.60 (s, 1H, –C=CH), 5.49 (s, 2H, CH_2), 5.46 (s, 2H, CH_2), 2.44 (s, 3H, CH_3), 2.41 (s, 3H, CH_3). ^{13}C NMR (75 MHz, DMSO-d_6) δ 160.24, 157.73, 150.63, 146.37, 142.93, 141.06, 138.84, 137.73, 133.42, 132.94, 131.63, 127.58, 126.37, 126.31, 124.76, 124.00, 123.20, 122.63, 121.20, 117.50, 117.41, 114.27, 112.84, 111.26, 52.57, 37.15, 21.27, 18.36. LC-MS (ESI) m/z 555.11 $[M+H]^+$; HRMS (ESI) calculated for $C_{28}H_{23}BrN_6O_2$ $[M+H]^+$ 555.1165, found 555.1144.

6-Bromo-1-((1-(3-(5,6-dimethyl-1*H*-benzo[d]imidazol-2-yl)-4-hydroxybenzyl)-1*H*-1,2,3-triazol-4-yl)methyl)-4-methylquinolin-2(1*H*)-one (7c)

Yield 56%, off-white solid, Rf: 0.23 (CH_2Cl_2/CH_3OH: 9.85/0.15), Mp (°C) 288-290, UV (CH_2Cl_2/CH_3OH: 1/1) λmax = 214, 326 nm, ^{1}H NMR (300 MHz, DMSO-d_6) δ 13.38 (s, 1H, OH), 13.05 (s, 1H, NH), 8.08 (d, J = 5.8 Hz, 2H, Ar-H), 7.95 (s, 1H, Ar-H), 7.74 (dd, J = 22.7, 9.0 Hz, 2H, Ar-H), 7.53 (s, 1H, triazole-CH), 7.45 – 7.33 (m, 2H, Ar-H), 7.05 (d, J = 8.4 Hz, 1H, Ar-H), 6.67 (s, 1H, –C=CH), 5.55 (s, 2H, CH_2), 5.53 (s, 2H, CH_2), 2.48 (s, 3H, CH_3), 2.40 (s, 6H, 2×CH_3). ^{13}C NMR (75 MHz, CDCl3) δ 160.84, 158.30, 150.77, 146.99, 143.54, 140.02, 138.31, 133.56, 132.80, 132.08, 128.19, 126.84, 123.80, 123.21, 121.79, 118.48, 118.09, 117.98, 114.88, 113.50, 112.05, 53.18, 37.74, 20.56, 18.98, some peaks are overlapping. LC-MS (ESI) m/z 569.13 $[M+H]^+$; HRMS (ESI) calculated for $C_{29}H_{25}BrN_6O_2$ $[M+H]^+$ 569.1286, found 569.1295.

6-Bromo-1-((1-(3-(5-fluoro-1*H*-benzo[d]imidazol-2-yl)-4-hydroxybenzyl)-1*H*-1,2,3-triazol-4-yl)methyl)-4-methylquinolin-2(1*H*)-one (7d)

Yield 53%, white solid, Rf: 0.21 (CH_2Cl_2/CH_3OH: 9.85/0.15), Mp (°C) 276-278, UV (CH_2Cl_2/CH_3OH: 1/1) λmax = 237, 322 nm, ^{1}H NMR (300 MHz, DMSO-d_6) δ 13.21 (s, 1H, OH),

12.81 (s, 1H, NH), 8.06 (d, J = 1.9 Hz, 1H, Ar-H), 8.02 (s, 1H, Ar-H), 7.86 (d, J = 2.1 Hz, 1H, Ar-H), 7.75 – 7.63 (m, 2H, Ar-H), 7.61 (s, 1H, triazole-CH), 7.55 – 7.39 (m, 1H, Ar-H), 7.35 (dd, J = 8.5, 1.6 Hz, 1H, Ar-H), 7.12 (m, 1H, Ar-H), 7.02 (d, J = 8.4 Hz, 1H, Ar-H), 6.59 (s, 1H, –C=CH), 5.50 (s, 2H, CH_2), 5.46 (s, 2H, CH_2), 2.40 (s, 3H, CH_3). ^{13}C NMR (75 MHz, DMSO-d_6) δ 160.23, 157.52, 152.41, 146.36, 142.94, 137.72, 132.93, 132.00, 131.85, 130.05, 127.57, 126.80, 126.53, 123.22, 122.62, 121.20, 119.06, 118.93, 117.47, 114.26, 112.89, 52.49, 37.15, 18.35, some peaks are overlapping. LC-MS (ESI) m/z 559.09 $[M+H]^+$; HRMS (ESI) calculated for $C_{27}H_{20}BrFN_6O_2$ $[M+H]^+$ 559.0888, found 559.0886.

6-Bromo-1-((1-(4-hydroxy-3-(5-(trifluoromethyl)-1*H*-benzo[d]imidazol-2-yl) benzyl)-1*H*-1,2,3-triazol-4-yl)methyl)-4-methylquinolin-2(1*H*)-one (7e)

Yield 66%, white solid, Rf: 0.21 (CH_2Cl_2/CH_3OH: 9.85/0.15), Mp (°C) 286-288, UV (CH_2Cl_2/CH_3OH: 1/1) λmax = 236, 293, 331 nm, ^{1}H NMR (300 MHz, DMSO-d_6) δ 13.39 (s, 1H,OH), 12.55 (s, 1H, NH), 8.12 (s, 1H, Ar-H), 8.03 (s, 1H, Ar-H), 7.89 (m, 2H, Ar-H), 7.79 (d, J = 8.4 Hz, 1H, Ar-H), 7.71 (dd, J = 9.0, 2.2 Hz, 1H), 7.65 (s, 1H, triazole-CH), 7.63 – 7.56 (m, 1H, Ar-H), 7.38 (dd, J = 8.5, 2.0 Hz, 1H, Ar-H), 7.05 (d, J = 8.5 Hz, 1H, Ar-H), 6.60 (s, 1H, –C=CH), 5.52 (s, 2H, CH_2), 5.47 (s, 2H, CH_2), 2.41 (s, 3H, CH_3).^{13}C NMR (75 MHz, DMSO-d_6) δ 160.23, 157.46, 153.02, 146.37, 142.93, 137.72, 132.94, 132.41, 127.58, 127.38, 126.74, 123.25, 122.63, 121.20, 119.62, 118.84, 117.49, 115.45, 114.25, 112.87, 112.66, 52.41, 37.15, 18.35, some peaks are overlapping. LC-MS (ESI) m/z 609.08 $[M+H]^+$; HRMS (ESI) calculated for $C_{28}H_{20}BrF_3N_6O_2$ $[M+H]^+$ 609.0883, found 609.0863.

6-Bromo-1-((1-(3-(5-chloro-1*H*-benzo[d]imidazol-2-yl)-4-hydroxybenzyl)-1*H*-1,2,3-triazol-4-yl)methyl)-4-methylquinolin-2(1*H*)-one (7f)

Yield 70%, white solid, Rf: 0.2 (CH_2Cl_2/CH_3OH: 9.85/0.15), Mp (°C) 278-280, UV (CH_2Cl_2/CH_3OH: 1/1) λmax = 236, 293, 331 nm, ^{1}H NMR (300 MHz, DMSO-d_6) δ 13.23 (s, 1H, OH), 12.79 (s, 1H, NH), 8.12 (d, J = 1.9 Hz, 1H,Ar-H), 8.07 (s, 1H, Ar-H), 7.89 (d, J = 2.1 Hz, 1H, Ar-H), 7.74 (dd, J = 9.0, 2.1 Hz, 2H, Ar-H), 7.69 – 7.66 (m, 1H, Ar-H), 7.68 (s, 1H, triazole-CH), 7.41 (dd, J = 8.5, 1.9 Hz, 1H, Ar-H), 7.32 (dd, J = 8.6, 1.7 Hz, 1H, Ar-H), 7.07 (d, J = 8.5 Hz, 1H, Ar-H), 6.63 (s, 1H,–C=CH), 5.55 (s, 2H, CH_2), 5.50 (s, 2H, CH_2), 2.44 (s, 3H, CH_3).^{13}C NMR (75 MHz, DMSO-d_6) δ 160.93, 158.39, 152.88, 146.60, 143.63, 138.64, 133.38, 132.52, 128.05, 127.89, 127.47, 126.98, 123.72, 123.54, 123.40, 121.96, 118.13, 117.97, 114.79, 113.57, 53.34, 37.98, 18.68, some peaks are overlapping. LC-MS (ESI) m/z 575.06 $[M+H]^+$; HRMS (ESI) calculated for $C_{27}H_{20}BrClN_6O_2$ $[M+H]^+$ 575.0592, found 575.0580.

6-Bromo-1-((1-(3-(5-bromo-1*H*-benzo[d]imidazol-2-yl)-4-hydroxybenzyl)-1*H*-1,2,3-triazol-4-yl)methyl)-4-methylquinolin-2(1*H*)-one (7g)

Yield 60%, white solid, Rf: 0.2 (CH_2Cl_2/CH_3OH: 9.85/0.15), Mp (°C) 250-252, UV (CH_2Cl_2/CH_3OH: 1/1) λmax = 221, 278, 324 nm, ^{1}H NMR (300 MHz, DMSO-d_6) δ 13.20 (s, 1H, OH), 12.67 (s, 1H, NH), 8.06 (d, J = 1.8 Hz, 1H, Ar-H), 8.00 (s, 1H, Ar-H), 7.92 – 7.76 (m, 2H, Ar-H), 7.68 (dd, J = 9.0, 2.0 Hz, 1H,Ar-H), 7.62 (s, 1H, triazole-CH), 7.59 (s, 1H,Ar-H), 7.42 – 7.30 (m, 2H,Ar-H), 7.01 (d, J = 8.4 Hz, 1H,Ar-H), 6.57 (s, 1H,–C=CH), 5.49 (s, 2H, CH_2), 5.44 (s, 2H, CH_2), 2.38 (s, 3H, CH_3). ^{13}C NMR (75 MHz, DMSO-d_6) δ 160.90, 158.33, 152.68, 146.66, 143.60, 138.63, 133.43, 132.59, 128.10, 127.55, 127.06, 126.18, 123.73, 123.39, 121.96, 118.12, 118.03, 115.48, 114.77, 113.54, 53.28, 37.95, 18.74, some peaks are overlapping. LC-MS (ESI) m/z 619.01 $[M+H]^+$; HRMS (ESI) calculated for $C_{27}H_{20}Br_2N_6O_2$ $[M+H]^+$ 619.0087, found 619.0079.

1-((1-(3-(1*H*-benzo[d]imidazol-2-yl)-4-hydroxybenzyl)-1*H*-1,2,3-triazol-4-yl)methyl)-6-fluoro-4-methylquinolin-2(1*H*)-one (7h)

Yield 76%, white solid, Rf: 0.19 (CH_2Cl_2/CH_3OH: 9.85/0.15), Mp (°C) 276-278, UV (CH_2Cl_2/CH_3OH: 1/1) λmax = 218, 333 nm, ^{1}H NMR (300 MHz, DMSO-d_6) δ 13.20 (s, 2H, OH+NH), 8.07 (s, 1H, Ar-H), 8.02 (s, 1H, Ar-H), 7.71 (dd, J = 9.3, 4.6 Hz, 2H, Ar-H), 7.61 (brs, 1H, Ar-H), 7.53 (dd, J = 9.7, 2.8 Hz, 1H, Ar-H), 7.44 (td, J = 8.6, 2.8 Hz, 1H, Ar-H), 7.35 (d, J = 8.5 Hz, 1H, Ar-H), 7.27 (d, J = 4.6 Hz, 2H,Ar-H), 7.01 (d, J = 8.4 Hz, 1H,Ar-H), 6.60 (s, 1H,–C=CH), 5.50 (s, 2H, CH_2), 5.47 (s, 2H, CH_2), 2.37 (s, 3H, CH_3).^{13}C NMR (75 MHz, DMSO-d_6) δ 160.85, 159.31, 157.73 (d, J_{C-F} = 239.2 Hz), 151.61, 147.14 (d, J_{C-F} = 3.1 Hz), 143.71, 141.33, 135.88, 133.80, 132.45, 127.20, 127.02, 123.85, 123.03, 122.55 (d, J_{C-F} = 8.2 Hz), 121.84, 118.60 (d, J_{C-F} = 23.7 Hz), 118.07, 117.77 (d, J_{C-F} = 8.3 Hz), 113.38, 112.24, 111.45 (d, J_{C-F} = 23.1 Hz), 53.15, 37.85, 19.04. LC-MS (ESI) m/z 481.18 $[M+H]^+$; HRMS (ESI) calculated for $C_{27}H_{21}FN_6O_2$ $[M+H]^+$ 481.1783, found 481.1782.

6-Fluoro-1-((1-(4-hydroxy-3-(5-methyl-1*H*-benzo[d]imidazol-2-yl)benzyl)-1*H*-1,2,3-triazol-4-yl)methyl)-4-methylquinolin-2(1*H*)-one (7i)

Yield 75%, white solid, Rf: 0.21 (CH_2Cl_2/CH_3OH: 9.85/0.15), Mp (°C) 240-242, UV (CH_2Cl_2/CH_3OH: 1/1) λmax = 226, 276, 324 nm,^{1}H NMR (300 MHz, DMSO-d_6) δ 13.24 (s, 1H, OH), 13.11 (s, 1H, NH), 8.05 (s, 1H, Ar-H), 8.02 (s, 1H, Ar-H), 7.72 (dd, J = 9.2, 4.6 Hz, 1H, Ar-H), 7.56 (dd, J = 9.7, 2.5 Hz, 2H, Ar-H), 7.45 (m, 2H, Ar-H), 7.39 – 7.30 (m, 1H, Ar-H), 7.09 (d, J = 6.3 Hz, 1H, Ar-H), 7.00 (d, J = 8.5 Hz, 1H, Ar-H), 6.62 (s, 1H, –C=CH), 5.50 (s, 2H, CH_2), 5.48 (s, 2H, CH_2), 2.44 (s, 3H, CH_3), 2.39 (s, 3H, CH_3).^{13}C NMR (75 MHz, DMSO-d_6) δ 160.96, 158.55, 157.88 (d, J_{C-F} = 239.6 Hz), 151.49, 146.80 (d, J_{C-F} = 3.1 Hz), 143.79, 136.24 (d, J_{C-F} = 1.5 Hz), 132.97, 132.02,

126.97, 126.72, 124.88, 123.67, 122.76 (d, J_{C-F} = 8.1 Hz), 122.03, 118.34 (d, J_{C-F} = 23.7 Hz), 118.01, 117.72 (d, J_{C-F} = 8.2 Hz), 113.74, 111.22 (d, J_{C-F} = 23.3 Hz), 53.42, 38.11, 21.68, 18.74, some peaks are overlapping. LC-MS (ESI) m/z 495.19 $[M+H]^+$; HRMS (ESI) calculated for $C_{28}H_{23}FN_6O_2$ $[M+H]^+$ 495.1939, found 495.1944.

1-((1-(3-(5,6-Dimethyl-1*H*-benzo[d]imidazol-2-yl)-4-hydroxybenzyl)-1*H*-1,2,3-triazol-4-yl)methyl)-6-fluoro-4-methylquinolin-2(1*H*)-one (7j)

Yield 78%, off white solid, Rf: 0.11 (CH_2Cl_2/CH_3OH: 9.85/0.15), Mp (°C) 288-290, UV (CH_2Cl_2/CH_3OH: 1/1) λmax = 220, 276, 326 nm, ^{1}H NMR (300 MHz, DMSO-d_6) δ 8.00 (d, J = 2.1 Hz, 1H, Ar-H), 7.88 (s, 1H, Ar-H), 7.73 (dd, J = 9.3, 4.7 Hz, 1H, Ar-H), 7.50 (dd, J = 9.7, 2.9 Hz, 1H, Ar-H), 7.43 – 7.34 (m, 3H, Ar-H), 7.28 (dd, J = 8.5, 2.1 Hz, 1H, Ar-H), 6.97 (d, J = 8.4 Hz, 1H, Ar-H), 6.58 (s, 1H, –C=CH), 5.49 (s, 2H, CH_2), 5.49 (s, 2H, CH_2), 2.40 (s, 3H, CH_3), 2.36 (s, 6H, 2×CH_3). ^{13}C NMR (75 MHz, DMSO-d_6) δ 160.96, 158.54, 157.88 (d, J_{C-F} = 239.6 Hz), 150.99, 146.79 (d, J_{C-F} = 3.1 Hz), 143.78, 136.24, 132.05, 131.84, 126.83, 126.62, 123.66, 122.76 (d, J_{C-F} = 8.0 Hz), 122.03, 118.34 (d, J_{C-F} = 23.8 Hz), 117.97, 117.72 (d, J_{C-F} = 8.2 Hz), 113.82, 111.22 (d, J_{C-F} = 23.2 Hz), 53.44, 38.11, 20.23, 18.74, some peaks are overlapping. LC-MS (ESI) m/z 509.21 $[M+H]^+$; HRMS (ESI) calculated for $C_{29}H_{25}FN_6O_2$ $[M+H]^+$ 509.2096, found 509.2091.

6-Fluoro-1-((1-(3-(5-fluoro-1*H*-benzo[d]imidazol-2-yl)-4-hydroxybenzyl)-1*H*-1,2,3-triazol-4-yl)methyl)-4-methylquinolin-2(1*H*)-one (7k)

Yield 69%, white solid, Rf: 0.23 (CH_2Cl_2/CH_3OH: 9.85/0.15), Mp (°C) 259-261, UV (CH_2Cl_2/CH_3OH: 1/1) λmax = 218, 275, 322 nm, ^{1}H NMR (300 MHz, DMSO-d_6) δ 13.26 (s, 1H, OH), 12.85 (s, 1H, NH), 8.11 (d, J = 2.1 Hz, 1H, Ar-H), 8.06 (s, 1H, Ar-H), 7.75 (dd, J = 9.3, 4.7 Hz, 1H, Ar-H), 7.68 (s, 1H,Ar-H), 7.59 (dd, J = 9.7, 2.9 Hz, 1H, Ar-H), 7.55 – 7.43 (m, 2H, Ar-H), 7.39 (dd, J = 8.5, 2.1 Hz, 1H, Ar-H), 7.16 (t, J = 8.6 Hz, 1H, Ar-H), 7.06 (d, J = 8.5 Hz, 1H, Ar-H), 6.65 (s, 1H, –C=CH), 5.54 (s, 2H, CH_2), 5.51 (s, 2H, CH_2), 2.42 (s, 3H, CH_3).^{13}C NMR (75 MHz, DMSO-d_6) δ 160.23, 157.45, 157.12 (d, J = 239.2 Hz), 152.01, 146.54 (d, J = 3.1 Hz), 143.09, 135.28, 131.95, 126.82, 126.54, 123.25, 121.94 (d, J = 8.2 Hz), 1201.23, 118.00 (d, J = 23.7 Hz), 117.45, 117.16 (d, J = 8.4 Hz), 112.89, 110.85 (d, J = 23.0 Hz), 52.48, 37.24, 18.43, some peaks are overlapping. LC-MS (ESI) m/z 499.17 $[M+H]^+$; HRMS (ESI) calculated for $C_{27}H_{20}F_2N_6O_2$ $[M+H]^+$ 499.1715, found 499.1696.

6-Fluoro-1-((1-(4-hydroxy-3-(5-(trifluoromethyl)-1*H*-benzo[d]imidazol-2-yl)benzyl)-1*H*-1,2,3-triazol-4-yl)methyl)-4-methylquinolin-2(1*H*)-one (7l)

Yield 74%, white solid, Rf: 0.23 (CH_2Cl_2/CH_3OH: 9.85/0.15), Mp (°C) 268-270, UV (CH_2Cl_2/CH_3OH: 1/1) λmax = 221, 293, 331 nm, ^{1}H NMR (300 MHz, DMSO-*d*$_6$) δ 13.40 (s, 1H, OH), 8.13 (s, 1H,Ar-H), 8.04 (s, 1H, Ar-H), 7.82 (s, 1H, Ar-H), 7.71 (dd, J = 9.3, 4.7 Hz, 1H, Ar-H), 7.61 – 7.49 (m, 2H, Ar-H), 7.49 – 7.36 (m, 2H, Ar-H), 7.05 (d, J = 8.5 Hz, 2H, Ar-H), 6.60 (s, 1H, –C=CH), 5.52 (s, 2H, CH_2), 5.47 (s, 2H, CH_2), 2.38 (s, 3H, CH_3).^{13}C NMR (75 MHz, DMSO-*d*$_6$) δ 160.96, 158.49, 157.88 (d, J_{C-F} = 239.7 Hz), 154.08, 146.72 (d, J_{C-F} = 3.1 Hz), 143.83, 136.25 (d, J_{C-F} = 1.4 Hz), 132.83, 130.91, 127.83, 127.31, 127.12, 124.27 (q, J_{C-F} = 31.8 Hz), 123.73 (s, J_{C-F} = 6.4 Hz), 122.76 (d, J_{C-F} = 8.1 Hz), 122.03, 120.11, 119.85 (q, J_{C-F} = 3.6 Hz), 118.28 (d, J_{C-F} = 23.8 Hz), 118.22, 117.67 (d, J_{C-F} = 8.2 Hz), 113.57, 111.16 (d, J_{C-F} = 23.2 Hz), 53.32, 38.13, 18.67, some peaks are overlapping. LC-MS (ESI) m/z 549.17 $[M+H]^+$; HRMS (ESI) calculated for $C_{28}H_{20}F_4N_6O_2$ $[M+H]^+$ 549.1657, found 549.1661.

1-((1-(3-(5-Chloro-1*H*-benzo[d]imidazol-2-yl)-4-hydroxybenzyl)-1*H*-1,2,3-triazol-4-yl)methyl)-6-fluoro-4-methylquinolin-2(1*H*)-one (7m)

Yield 83%, white solid, Rf: 0.2 (CH_2Cl_2/CH_3OH: 9.85/0.15), Mp (°C) 245-247, UV (CH_2Cl_2/CH_3OH: 1/1) λmax = 224, 275, 323 nm, ^{1}H NMR (300 MHz, DMSO-*d*$_6$) δ 13.28 (s, 1H, OH), 12.74 (s, 1H, NH), 8.13 (s, 1H, Ar-H), 8.07 (s, 1H, Ar-H), 7.85 – 7.71 (m, 2H, Ar-H), 7.67 (s, 1H, Ar-H), 7.59 (d, J = 9.7 Hz, 1H, Ar-H), 7.51 (m, 1H, Ar-H), 7.41 (d, J = 8.4 Hz, 1H, Ar-H), 7.37 – 7.27 (m, 1H, Ar-H), 7.07 (d, J = 8.4 Hz, 1H, Ar-H), 6.66 (s, 1H, –C=CH), 5.55 (s, 2H, CH_2), 5.52 (s, 2H, CH_2), 2.43 (s, 3H, CH_3).^{13}C NMR (75 MHz, DMSO-*d*$_6$) δ 160.22, 157.46, 157.11 (d, J_{C-F} = 239.2 Hz), 152.10, 146.52 (d, J_{C-F} = 3.1 Hz), 143.07, 135.26, 132.11, 127.07, 126.59, 123.23, 122.61, 121.93 (d, J_{C-F} = 8.2 Hz), 121.22, 119.28, 117.99 (d, J_{C-F} = 23.7 Hz), 117.46, 117.14 (d, J_{C-F} = 8.1 Hz), 112.85, 111.38, 110.83 (d, J_{C-F} = 23.2 Hz), 52.45, 37.23, 18.42, some peaks are overlapping. LC-MS (ESI) m/z 515.14 $[M+H]^+$; HRMS (ESI) calculated for $C_{27}H_{20}ClFN_6O_2$ $[M+H]^+$ 515.1420, found 515.1400.

1-((1-(3-(5-Bromo-1*H*-benzo[d]imidazol-2-yl)-4-hydroxybenzyl)-1*H*-1,2,3-triazol-4-yl)methyl)-6-fluoro-4-methylquinolin-2(1*H*)-one (7n)

Yield 59%, white solid, Rf: 0.2 (CH_2Cl_2/CH_3OH: 9.85/0.15), Mp (°C) 277-279, UV (CH_2Cl_2/CH_3OH: 1/1) λmax = 224, 275, 323 nm, ^{1}H NMR (300 MHz, DMSO-*d*$_6$) δ 13.20 (s, 1H, OH), 12.71 (s, 1H, NH), 8.08 (s, 1H, Ar-H), 8.02 (s, 1H, Ar-H), 7.83 (s, 1H, Ar-H), 7.71 (dd, J = 9.0, 4.5 Hz, 1H), 7.64 – 7.48 (m, 2H, Ar-H), 7.49 – 7.41 (m, 1H, Ar-H), 7.40 – 7.30 (m, 2H, Ar-H), 7.02 (d, J = 7.8 Hz, 1H, Ar-H), 6.60 (s, 1H, –C=CH), 5.50 (s, 2H, CH_2), 5.47 (s, 2H, CH_2), 2.38 (s, 3H, CH_3). ^{13}C NMR (75 MHz, DMSO-*d*$_6$) δ 160.22, 157.47, 157.11 (d, J_{C-F} = 239.2 Hz), 151.84, 146.52 (d, J_{C-F} = 3.0 Hz), 143.07, 135.26, 132.13, 127.10, 126.60, 125.62, 123.24, 121.93 (d, J_{C-F} = 8.2 Hz), 121.22,

117.98 (d, J_{C-F} = 23.8 Hz), 117.46, 117.14 (d, J_{C-F} = 8.3 Hz), 112.83, 110.83 (d, J_{C-F} = 23.0 Hz), 52.45, 37.23, 18.42, some peaks are overlapping. LC-MS (ESI) m/z 561.09 $[M+H]^+$; HRMS (ESI) calculated for $C_{27}H_{20}BrFN_6O_2$ $[M+H]^+$ 559.0888, found 559.0877.

2.2. Single crystal X-ray diffraction

Suitable crystals of compounds **6b** and **7a** were grown by slow evaporation from their dichloromethane/methanol and dichloromethane/DMSO solutions, respectively, at ambient temperature. Crystal evaluation and data collection for these compounds were performed at 173 K on a Bruker Venture diffractometer with a Mo-Kα microsource and equipped with a Photon-II detector. The APEX3 program was used for data collection and SAINT, XPREP and SADABS for the integration of the data using default parameters, for the empirical absorption correction using spherical harmonics employing symmetry-equivalent and redundant data, and the correction for Lorentz and polarization effects [37]. The frames were integrated with the Bruker SAINT software package using a narrow-frame algorithm. The two crystal structures were solved using the ab initio iterative charge flipping method with parameters described elsewhere [38] using the Superflip program [39]. The structural models were refined against $|F|^2$ using full-matrix non-linear least-squares procedures as implemented in CRYSTALS [40] on all independent reflections with $I>-3\sigma(I)$. The hydrogen atoms were refined with riding constraints in all structures [41].

2.3. Biology

Antibacterial testing of all compounds (**6a,b** and **7a-c**) was carried out against *Staphylococcus aureus* (CIP 53154) and *Escherichia coli* (CIP 54127) by the micro-broth dilution method in 96-well plates according to the Clinical and Laboratory Standards Institute (CLSI) guidelines M07-A10 for bacteria [42]. Each bacterial suspension was prepared from a colony of each strain culture in sterile physiological water (NaCl solution at 0.9%), and then adjusted to 108 CFU/mL at 620 nm equivalent to 0.5 McFarland. Test compounds were dissolved in chloroform/DMSO (1:1) which was used as a negative control, while ampicillin was used as a positive control. Plates were incubated at 37 °C for 24 h. The lowest concentration that prevents visible growth of the bacterial strains was regarded as minimum inhibitory concentrations (MIC). The minimum bactericidal concentration (MBC) was recorded as the lowest concentration that kills at least 99.99% of bacteria. All experiments were performed in duplicate.

2.4. Computational details

The quantum chemical calculations were performed by means of the Gaussian 09Wprogram [43,44] package with the Density Functional Theory (DFT) using the hybrid functional B3LYP functional

[45,46] and the basis set 6-31+G (d,p). Geometric optimizations were performed in the gas phase and all structures have no imaginary frequencies; this state means that they are being at global minima on the total potential energy surface (PES). The chemical reactivity parameters, namely, energy gap (Eg), ionization energy (I), electron affinity (A), chemical potential (μ), global hardness (η), electronegativity (χ) and electrophilicity index (ω) were calculated based on the Koopmans' theorem [47] *via* the following equations (1) - (7) :

$$Eg = E_{LUMO} - E_{HOMO} \quad (1)$$

$$I = - E_{LUMO} \quad (2)$$

$$A = - E_{HOMO} \quad (3)$$

$$\mu = (E_{LUMO} + E_{HOMO})/ 2 \quad (4)$$

$$\eta = (E_{LUMO} - E_{HOMO})/ 2 \quad (5)$$

$$\chi = -\mu \quad (6)$$

$$\omega = \mu^2/2\eta \quad (7)$$

2.5. Molecular docking

The crystal structure of DNA gyrase A co-crystallized with ciprofloxacin (PDB ID: 2XCT) and DNA gyrase B co-crystallized with 4-methyl-5-[3-(methylsulfanyl)-1*H*-pyrazol-5-yl]-2-thiophen-2-yl-1,3-thiazole (PDB ID: 3G75) of *S. aureus* were retrieved from protein data bank (PDB) (Source: www.rcsb.org/pdb/). The proteins were prepared by deleting water molecules and native ligands. Then they were saved in PDBQT format after adding Kollman and Gastieger charges and polar hydrogens using AutoDockTools-1.5.7 software. The structures of the studied compounds were drawn using ChemDraw Ultra 12.0, energy minimized in Chem3D Ultra software using MM2 force field and saved in PDBQT format for input into docking. AutoDock Vina was used to execute the docking calculations [48]. The active site of 2XCT protein defined by a grid box size of 20 × 20 × 20 Å centered at (x, y, z) of (-12.8, 34.8, 65.8) Å was used for docking. As regards 3G75 protein, the grid box was generated at the binding pocket with a grid box size of 20 × 20 × 20 Å centered at (x, y, z) of (48.3, -4.3, 16.1) Å. The resulting docking conformations were analyzed with the Discovery Studio Visualizer v21.1.

3. Results and discussion

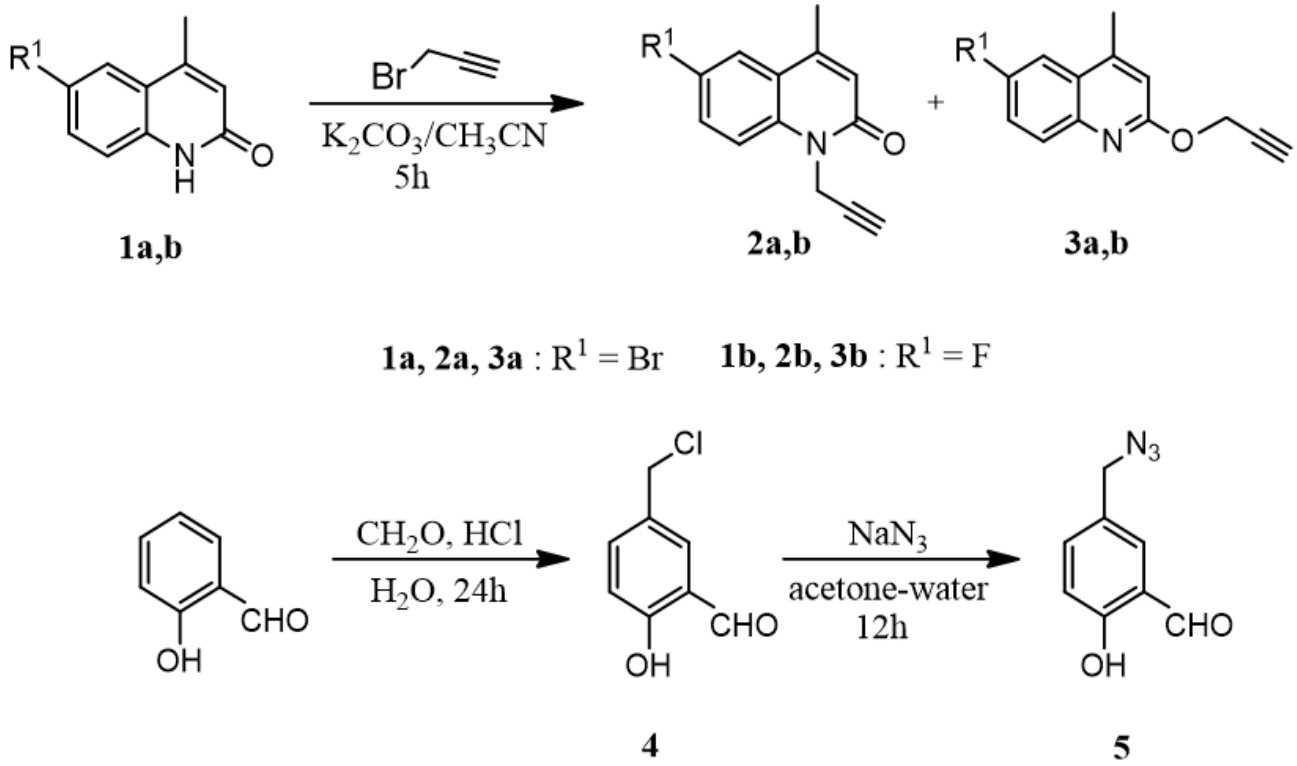

Scheme 1. Synthesis of starting compounds.

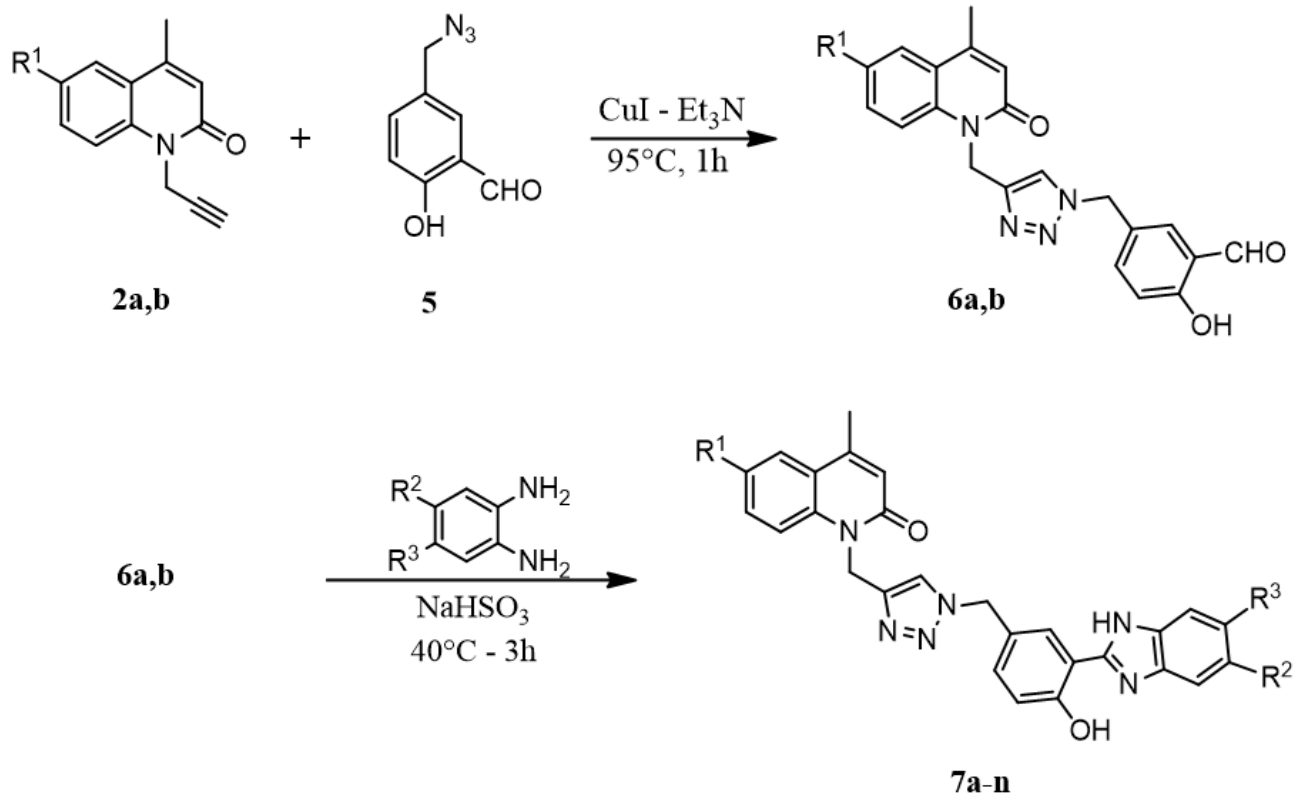

Scheme 2. Synthesis of novel hybrid compounds based on quinolin-2-one.

3.1. Chemistry

Initially, the starting materials 6-bromo-4-methylquinolin-2(1*H*)-one **1a** and 6-fluoro-4-methylquinolin-2(1*H*)-one **1b** were synthesized in a two-step sequence from ethyl acetoacetate and halogen-substituted aniline using Knorr reaction conditions according to the literature [49,50]. Next, compounds **1a,b** were reacted with propargyl bromide in the presence of K_2CO_3 to give a mixture of N- and O-alkylated products. N-propargylated quinolones **2a,b** were the major products (60-66%), while their O-regioisomers **3a,b** were formed in poor yields (17-19%) (Scheme 1).The precursor **4** was synthesized from salicylaldehyde following an already described method [35]. Then it converts in to the azido derivative **5** by reacting it with sodium azide (Scheme 1). This was followed by a Cu(I)-catalyzed azide-alkyne 1,3-dipolar cycloaddition (CuAAC) of the azide salicylaldehyde **5** with N-propargylated quinolones. The reactions were carried out in DMF in the presence of Et_3N and copper(I)-iodide leading to new 1,4-disubstituted 1,2,3-triazole-derived quinolones **6a,b** in high yields (80-93%) (Scheme 2). Finally, the condensation of the carbonyl group of the triazole derivatives **6a,b** with a variety of phenylenediamines afforded the corresponding benzimidazole hybrids **7a-n** in fair to good yields. The reaction took place in absolute ethanol/water at a temperature of 40°C with sodium bisulfite ($NaHSO_3$) as oxidant agent according to a reported method with some modification [36] (Scheme 2). $NaHSO_3$ was used as a catalyst to promote the oxidative cyclodehydrogenation of Schiff bases intermediates generated from the condensation reaction [51]. The choice of $NaHSO_3$ was due to its low-cost, chemoselectivity and low environmental impact. The results obtained were grouped in Table 1. The structures of all products were elucidated by LC-MS, HRMS and NMR spectroscopy. The structures of compounds **6b** and **7a** were additionally confirmed by single-crystal X-ray diffraction analysis.

3.2. Spectral analysis

The formation of 1,2,3-triazole-derived quinolones **6a,b** was confirmed by the NMR data. For instance, the ^{1}H NMR spectrum of compound **6a** showed a singlet at δ 7.53 ppm, which was assigned to -CH of triazole ring. The proton of aldehyde group -CHO appeared as singlet at δ 9.76 ppm, while the salicyl OH proton resonated at δ 10.96 ppm. In the ^{13}C NMR spectrum of compound **6a**, the signals of the carbon atoms of the 1,2,3-triazole moiety were observed at δ 125.92 and δ 144.05 ppm. Both methylene carbons -CH_2 exhibited peaks at δ 38.06 and δ 53.18 ppm. The conversion of compounds **6a,b** into benzimidazole derivatives **7a,n** was confirmed by the absence of the signal due to the proton of the formyl group in the ^{1}H NMR spectrum and, in the ^{13}C NMR spectrum, by the appearance of a signal due to the carbon atom attached to NH of the imidazole unit between δ 150.63 - 154.08 ppm. The peaks corresponding to OH (phenol) and NH (imidazole) protons were located in the

downfield region between δ 12,55 and δ 13,4 ppm, implying their involvement in the formation of hydrogen bonds, which was also evidenced by the density functional theory (DFT) calculations and X-ray diffraction analysis. This finding agreed with another report [52]. Worthy to note is that for some benzimidazole derivatives, NH and OH protons could merge together or they could undergo rapid proton exchange with the deuterated solvent, leading to the decrease or disappearance of the corresponding signals from the ^{1}H NMR spectra.

Mass analysis also supported the successful synthesis of the target molecules. The LC-MS and HRMS spectra of compound **6a**, as an example, revealed two molecular ion peaks at m/z 453 $[M+H]^+$ and m/z 455 $[M+H+2]^+$ due to the characteristic isotope pattern of bromine. The accurate mass of $[M+H]^+$ ion was m/z 453.0553, which was in complete accord with the calculated value for $C_{21}H_{17}{}^{79}BrN_4O_3$: 453.0557.

Table 1

Results of hybrid compounds **6a,b** and **7a-n.**

Entry	Product	R^1	R^2	R^3	Yield[a] (%)
1	**6a**	Br	-	-	80
2	**6b**	F	-	-	93
3	**7a**	Br	H	H	46
4	**7b**	Br	CH_3	H	56
5	**7c**	Br	CH_3	CH_3	56
6	**7d**	Br	F	H	53
7	**7e**	Br	CF_3	H	66
8	**7f**	Br	Cl	H	70
9	**7g**	Br	Br	H	60
10	**7h**	F	H	H	76
11	**7i**	F	CH_3	H	75
12	**7j**	F	CH_3	CH_3	77
13	**7k**	F	F	H	69
14	**7l**	F	CF_3	H	74
15	**7m**	F	Cl	H	73
16	**7n**	F	Br	H	59

[a] isolated yield

3.3. X-ray crystal structures description

The ORTEP-style drawings of **6b** and **7a** derivatives are illustrated in Fig. 2. Crystal data, data collection and structure refinement details are summarized in Table 2. A full check of the intramolecular geometry of the two compounds was performed using the MOGUL software [53,54]

against the data within the 5.43 version of the Cambridge Structural Database [55]: no unusual features were found in bond length, valence and torsion angles and ring geometries. Full crystallographic information can be obtained from the Cambridge Crystallographic Data Centre with the deposition numbers 2224015 (**6b**) and 2224016 (**7a**).

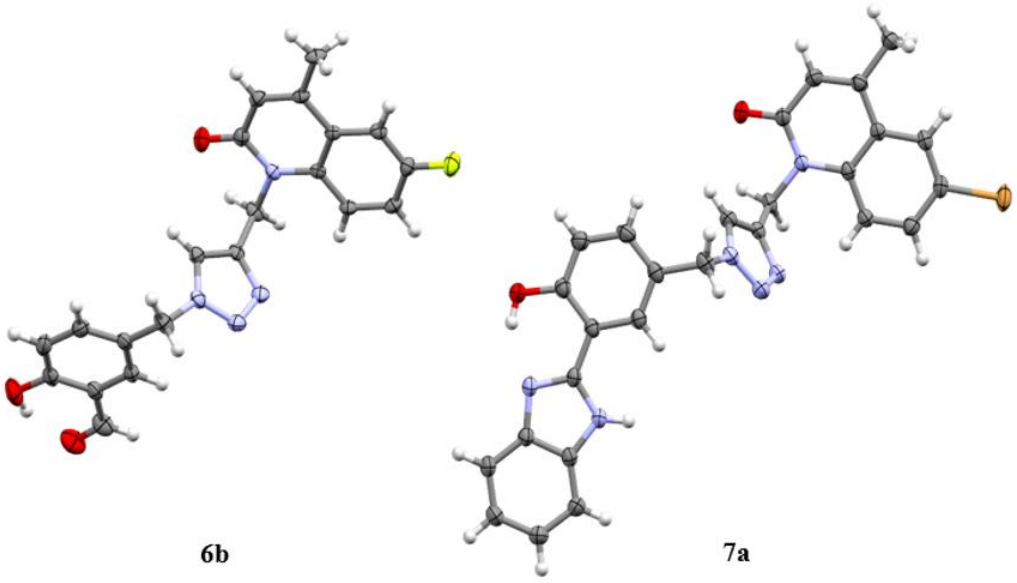

Fig. 2. ORTEP style drawings of the molecular structures of **6b** and **7a** based on the results from the X-ray diffraction analyses. The anisotropic atomic displacement ellipsoids have been drawn at the 50% probability level.

No classical intermolecular hydrogen bonds are present in the three-dimensional crystal structure of **6b**; however, there is an intramolecular hydrogen bond between the hydroxyl group and the carboxaldehyde group of the 2-hydroxybenzaldehyde scaffold. Molecules line up in linear chains along the *c*-*b* direction connected by relatively short π-π contacts (3.76 Å distance between centroids of adjacent fluorophenyl rings). These molecular chains line up in the *c*+*b* and *a* directions *via* other Van der Waals interactions, such as alkyl-π and anion-π interactions. A hydrogen-bond propensity analysis [56,57] of **6b** shows that the observed potential hydrogen-bond pattern with one donor and 5 acceptors, viz. no intermolecular hydrogen bonds, is exactly what is expected from a statistical comparison with structures with analogous donor and acceptor groups. In other words, if another polymorphic structure exists, it is likely to be less stable than the current structure.

Two hydrogen-bond interactions are present in the structure of **7a**: an intramolecular interaction between the phenolic hydrogen and the nitrogen atom of the benzimidazole ring, and an intermolecular one between the carbonyl oxygen of the quinolone scaffold of one moiety and the amino hydrogen of the benzimidazole unit of a neighboring moiety. The intermolecular hydrogen-bond contacts are

arranged in $C1^1(14)$ infinite chains along the crystallographic *a*-axis. Parallel molecular chains are connected to each other by different π type interactions, such as π-π and alkyl-π interactions, which are also found when this molecule interacts in the binding pockets of DNA gyrase A and DNA gyrase B of *S. aureus* with amino acid residues (see molecular docking study). A similar hydrogen-bond propensity analysis as for **6b** was performed, with for **7a** two possible donor groups and 6 possible acceptor groups, including Br. The observed hydrogen-bonding pattern is exactly what can be expected from the log it hydrogen-bonding propensity model derived from 1839 structures with analogous donor and acceptor sites, which leads to the conclusion that also this structure is the most stable polymorph for this compound.

Table 2

The crystal data and parameters for structure refinement of **6b** and **7a**.

Structure	**6b**	**7a**
Formula	$C_{21}H_{17}FN_4O_3$	$C_{27}H_{21}BrN_6O_2$
Moiety	$C_{21}H_{17}FN_4O_3$	$C_{27}H_{21}BrN_6O_2$
M_r (g.mol^{-1})	392.39	541.40
Temperature (K)	173	173
Crystal system	triclinic	triclinic
Space group	*P*-1	*P*-1
a (Å)	7.1544(12)	10.0981(4)
b (Å)	8.9067(14)	10.4977(5)
c (Å)	14.556(3)	12.5715(5)
α (°)	104.963(6)	80.962(2)
β (°)	90.363(6)	68.887(2)
γ (°)	98.997(6)	69.701(2)
V (Å^3)	884.0(3)	1165.21(9)
Z	2	2
P (g.cm^{-3})	1.474	1.543
μ (mm^{-1})	0.108	1.803
*R*int	0.068	0.093
θ_{max} (°)	36.387	29.651
Resolution (Å)	0.60	0.73
N_{tot} (measured)	67037	59705
N_{ref} (unique)	8574	6574
N_{ref} ($I > 2\sigma(I)$)	6241	4500
N_{ref} (least-squares)	8572	6573
N_{par}	266	333
$<\sigma(I)/I>$	0.0455	0.0496

R_1 ($I > 2\sigma(I)$)	0.0508	0.0393
wR_2 ($I>2\sigma(I)$)	0.1339	0.0904
R_1 (all)	0.0709	0.0692
wR_2 (all)	0.1506	0.1506
GOF	0.9995	0.9653
$\Delta\rho$ (min/max) (e Å^{-3})	-0.37/0.65	-0.76/0.69
crystal size mm^3	0.05x0.23x0.25	0.05x0.11x0.12

3.4. Biology

The *in vitro* activity of the newly synthesized compounds (**6a,b** and **7a-n**) was evaluated against Gram-negative bacterium strain *Escherichia coli* (CIP 53154) and Gram-positive bacterium strain *Staphylococcus aureus* (CIP 54127) and expressed as MIC and MBC values, which are summarized in Table 3. Ampicillin was selected as a standard antibiotic. In general, the tested molecules displayed moderate to high antibacterial activity. The triazole derivatives **6a** and **6b** exhibited modest levels of inhibitory activity. However, it was observed that the replacement of the bromine atom in position-6 of the quinolone moiety (compound **6a**) by the fluorine atom (compound **6b**) improved the activity against *S. aureus* by reducing the MIC and the MBC values from 11.03 to 3.19 µmol/mL. In addition, the fluoro derivative **6b** completely killed *E. coli* at MBC of 6.37 µmol/mL, while a concentration of 11.03 µmol/mL was required by the bromo derivative **6a** to completely kill the same bacterium. In case of compounds **7a-n**, the type of the substituent on the benzimidazole nucleus was found to have a significant effect on the biological activity. For hybrids containing 6-bromoquinolin-2-one core, compounds **7a**, **7c** and **7f** showed the highest activity. Compound **7a** having an unsubstituted benzimidazole ring and its dimethyl substituted analogue **7c** exerted remarkable selectivity toward *E. coli*. They had an MIC value of 0.14 µmol/mL, which was 1.85 times lower than that of the reference drug. Meanwhile, the MBCs of **7a** and **7c** were 0.29 µmol/mL and 0.27 µmol/mL, respectively, while the MBC of ampicillin was 0.53 µmol/mL. The chloro-modified derivative **7f** demonstrated excellent anti-staphylococcal activity with MIC and MBC values as low as 0.07 µmol/mL, which was 3.86-fold more potent than the control drug ampicillin. Furthermore, compound **7f** could effectively inhibit the growth of *E. coli* strain with an MIC of 0.14 µmol/mL. Noticeably, in the series of fluoroquinolin-2-one derivatives **7h-n**, the trifluoromethyl-bearing molecule **7l** gave the best antibacterial efficiencies with MIC and MBC values of 0.14 µmol/mL towards the two studied bacteria strains. The remaining compounds had weak to moderate inhibitory activity with MIC levels ranging from 0.32 to 10.11 µmol/mL for *S. aureus*, and 0.31 to 4.85 µmol/mL for *E. coli*, while the corresponding MBCs lay between 0.56 and 10.11 µmol/mL for *S. aureus*, and 0.31 and 9.71 µmol/mL for *E. coli*.

Considering the above, it can be concluded that the introduction of the benzimidazole scaffold generally increased the antibacterial activity. All the synthesized benzimidazole derivatives exhibited better efficacy than the corresponding 1,2,3-triazole hybrids, except for **7i** and **7n**, which had higher MICs against *S. aureus* in comparison to the parent **6b** (Fig. 3). The MBC/MIC ratios were calculated to determine whether the activity of the investigated 2-quinolone hybrids was bacteriostatic (MBC/MIC ratio > 4) or bactericidal (MBC/MIC ratio ≤ 4) [58]. Interestingly, the MBC/MIC ratios were ≤ 2, indicating the bactericidal effect of the tested compounds.

Table 3

Minimum inhibitory concentration (MIC in µmol/mL) and minimum bactericidal concentration (MBC in µmol/mL) of compounds **6a,b**, **7a-n** and standard drug ampicillin.

Compound	*S. aureus* (CIP 54127)			*E. coli* (CIP 53154)		
	MIC	MBC	MBC/MIC	MIC	MBC	MBC/MIC
6a	11.03	11.03	1	5.52	11.03	2
6b	3.19	3.19	1	6.37	6.37	1
7a	1.15	2.31	2	**0.14**	**0.29**	2
7b	0.56	0.56	1	4.5	4.5	1
7c	4.39	8.78	2	**0.14**	**0.27**	2
7d	2.23	2.23	1	0.56	0.56	1
7e	1.03	2.05	2	1.03	1.03	1
7f	**0.07**	**0.07**	1	**0.14**	**0.14**	1
7g	8.06	8.06	1	4.03	4.03	1
7h	0.32	0.65	2	0.32	0.65	2
7i	10.11	10.11	1	2.53	2.53	1
7j	2.46	4.92	2	0.61	0.61	1
7k	0.63	0.63	1	0.31	0.31	1
7l	**0.14**	**0.14**	1	**0.14**	**0.14**	1
7m	2.43	4.85	2	4.75	9.71	2
7n	4.47	4.47	1	4.47	4.47	1
Ampicillin	**0.27**	**0.27**	1	**0.26**	**0.53**	**2**

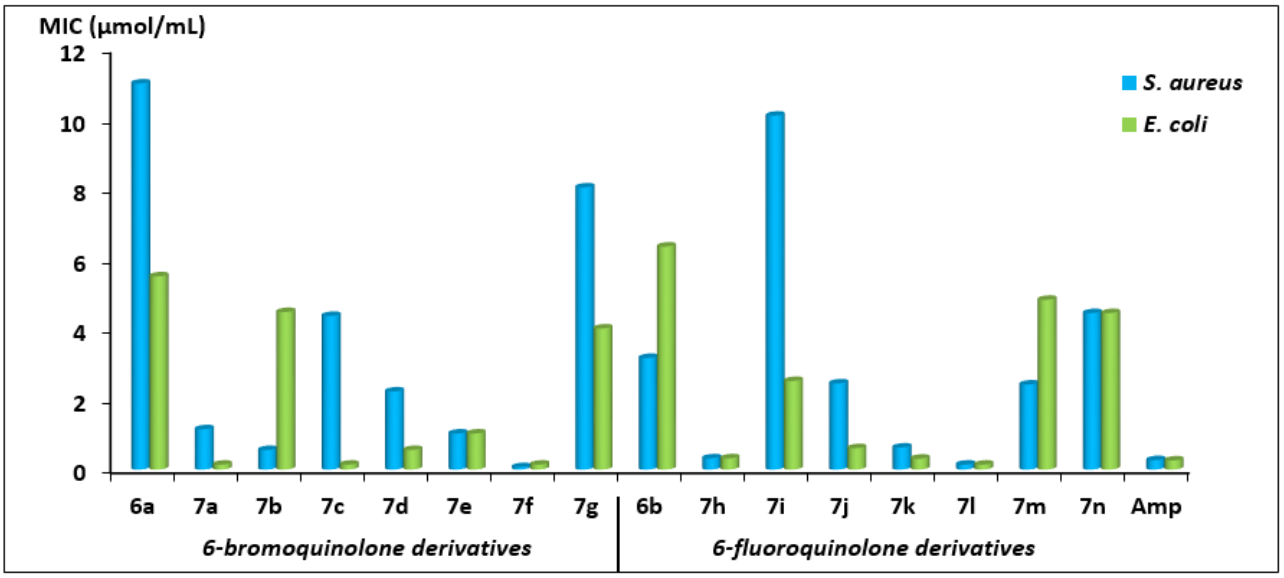

Fig. 3. Comparison of MICs (µmol/mL) of tested compounds (**6a,b** and **7a-n)** and ampicillin (Amp).

3.5. Computational studies

In order to support the biological results of compounds **7a**, **7c**, **7f** and **7l**, a computational study of their structural and electronic properties was undertaken using B3LYP /6-31+G (d,p) method.

3.5.1. Molecular structure study

Aided by DFT calculations, it was found that compounds **7a**, **7c**, **7f** and **7l** can exist as multiple conformational isomers. The first two lowest energy conformations of each compound were optimized in the isolated state (gaseous state) (Fig. 4, 5). The total and relative energies are gathered in Table 4, and the properties of the hydrogen bonds are reported in Table 5. The most stable conformation (the global minimum energy conformation) is the one that promotes the formation of two intramolecular hydrogen bonds of the type NH…O and OH…N. The first one is between the carbonyl oxygen (O_{18}) of the quinolone scaffold and the amino hydrogen (H_{46}) of the benzimidazole ring, and the second one is between the phenolic hydrogen (H_{42}) and the nitrogen atom (N_{44}) of the benzimidazole unit. This latter acts both as a donor and an acceptor making the molecule adopt a closed conformation (A) stabilized by the internal hydrogen bonds. The short calculated distances H_{46}…O_{18} (1.902-1.990 Å) and H_{42}…N_{44} (1.702-1.716 Å) demonstrated the strength of these bonds (Table 5).

Only the DFT optimized geometries of **7a** can be compared with the experimental X-ray structure, since only for this compound, single crystals of sufficient quality could be obtained for an X-ray diffraction data collection. The experimental structure has an open conformation as DFT structure **7a** (B), i.e. there is only one internal hydrogen bond, viz. between the phenolic hydrogen and the benzimidazole nitrogen atom. The root mean square difference (RMSD) between the experimental

molecular structure and the DFT structure **7a** (B) is 2.2633 Å, which can be considered as fairly large. The main difference lies in the relative orientation of the triazole moiety with respect to that of hydroxy-phenyl moiety, expressed as a nearly equal but opposite torsion angle difference through the C-CH_2-C segment joining the two moieties: 66.48° for the experimental structure **7a** and -66.05° for the DFT structure **7a** (B), so that the triazole-quinolone moiety in **7a** (B) is turned the same amount to the right as it is turned to the left in the experimental structure with respect to a perpendicular plane along the long axis of the benzimidazole unit. The RMSD between the experimental structure and the DFT structure **7a** (A) is larger with 3.4909 Å, meaning that the closed conformation of **7a** (A) is far from the more open conformation of the experimental structure.

The energy difference between conformers (A) and (B) is relatively small, in the interval of 1.46 - 4.1 kcal/mol, implying that the open structure (B) which has no hydrogen bond is also favorable. The open conformation is also more likely able to interact with a biological system through the formation of intermolecular hydrogen bonds in addition to hydrophobic and aromatic interactions. For this reason, conformers (B) were used in the ensuing calculations.

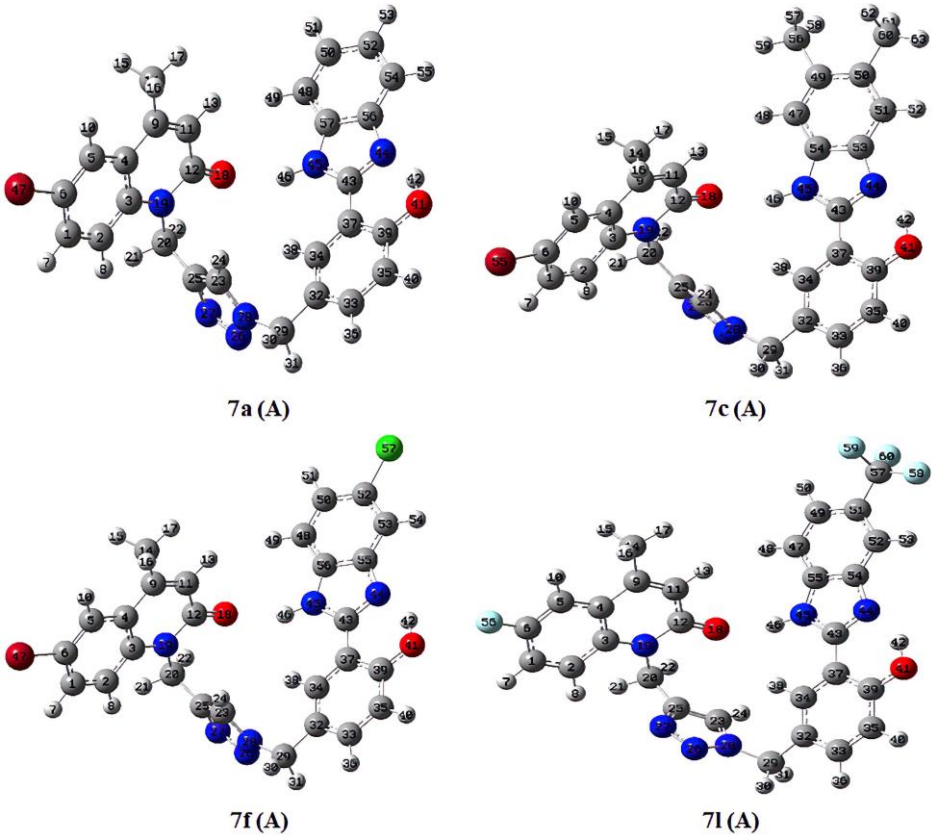

Fig. 4. DFT-optimized structures of conformers (A) of **7a**, **7c**, **7f** and **7l** in the gas phase.

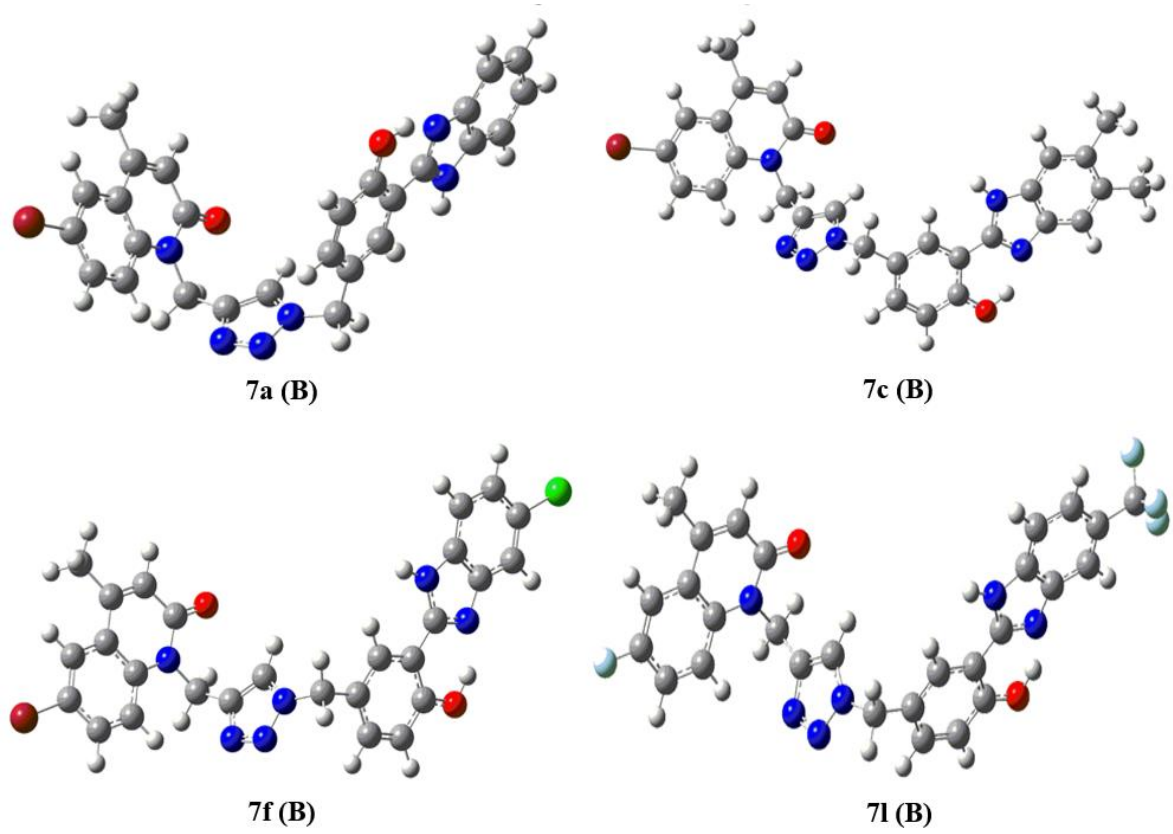

Fig. 5. DFT-optimized structures of conformers (B) of **7a**, **7c**, **7f** and **7l** in the gas phase.

Table 4

Total (E (a.u.)) and relative (ΔE (kcal/mol)) energies at B3LYP/6-31+G (d,p) level of low-lying isomers on the total PES of **7a**, **7c**, **7f** and **7l**.

Compound	E (a.u.)	ΔE (kcal/mol)
7a (A)	-4092.331993	1.72
7a (B)	-4092.329257	
7c (A)	-4170.971425	1,46
7c (B)	-4170.969105	
7f (A)	-4551.925809	2.50
7f (B)	-4551.921823	
7l (A)	-1957.506032	4.10
7l (B)	-1957.499505	

Table 5

Intramolecular hydrogen bonds parameters for conformations (A) of **7a**, **7c**, **7f** and **7l**.

Compound	D−H…A	D−H (Å)	H…A (Å)	D−H…A (°)
7a	N45—H46 … O18	1.019	1.977	158.407
	O41—H42 … N44	1.000	1.707	147.491
7c	N45—H46 … O18	1.018	1.990	158.409
	O41—H42 … N44	1.001	1.702	147.624
7f	N45—H46 … O18	1.019	1.962	158.083
	O41—H42 … N44	0.998	1.716	158.083
7l	N45—H46 … O18	1.024	1.902	164.525
	O41—H42 … N44	0.997	1.716	147.016

3.5.2. Frontier molecular orbital analysis

With the aim to get insight into the reactivity and the chemical stability of compounds **7a**, **7c**, **7f** and **7l**, the frontier molecular orbital analysis was carried out using the orbitals of HOMO (Highest Occupied Molecular Orbital) and LUMO (Lowest Unoccupied Molecular Orbital). The energies of these orbitals were utilized to calculate the energy gap (Eg) and the reactivity parameters (ionization energy (I), electron affinity (A), chemical potential (μ), global hardness (η), electronegativity (χ) and electrophilicity index (ω)) with the help of equations (1) - (7) given in the experimental section. The HOMO and LUMO of compounds **7a**, **7c**, **7f** and **7l** are displayed in Fig. 6, and the values of Eg, I, A, μ, χ and ω are listed in Table 6. The rearrangement of the atoms in the four molecules is the same regardless of the nature of the substituents (F, Cl, Br and CH_3). For hybrids **7a** and **7c**, the electron density of the HOMO is mainly located on the benzimidazole moiety and the phenolic group, while the LUMO is completely delocalized over on the quinolone ring. Contrastingly, for compounds **7f** and **7l,** the HOMO concentrates mostly on the quinolone scaffold, while the LUMO appears in the benzimidazole and the phenol rings. These results suggest that the intramolecular charge transfer occurs from the benzimidazole-phenol moiety to the quinolone part in compounds **7a** and **7c** and the opposite in compounds **7f** and **7l**. On the other hand, the distribution of frontier orbitals may have somehow contributed to the difference observed in the antibacterial activity between the four compounds, especially against *S. aureus*. Nevertheless, additional studies of molecular interactions would be required before concluding on this point.

As seen from Table 6, the energy gap (Eg) between the HOMO and LUMO orbitals is approximately 4.2 eV for compounds **7a**, **7f** and **7l** and 3 eV for compound **7c**. These values prove the good structural

stability of these molecules. Also, from the data of the global indexes, it is inferred overall that the investigated compounds could donate electrons to positively charged amino acid residues and accept free electrons when they interact with a biological environment.

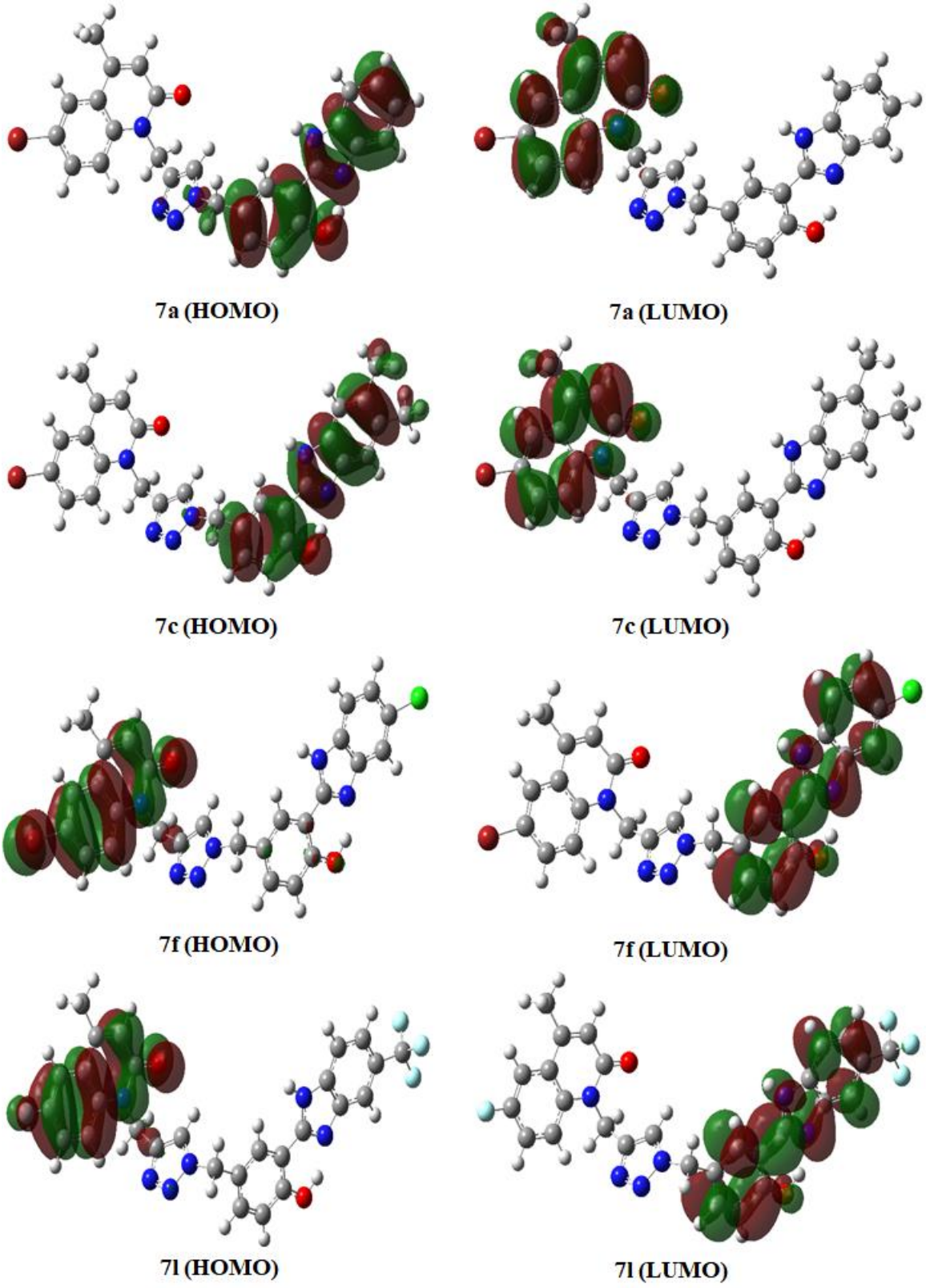

Fig. 6. HOMO-LUMO of **7a**, **7c**, **7f**, and **7l** compounds at B3LYP/6-31+G(d,p) level.

Table 6

HOMO-LUMO energies (eV) and calculated global reactivity parameters of compounds **7a**, **7c**, **7f** and **7l** at B3LYP/6-31+G(d,p) level in gas phase.

Compound	E_{HOMO} (eV)	E_{LUMO} (eV)	Eg (eV)	I (eV)	A (eV)	μ (eV)	η (eV)	X (eV)	ω (eV)
7a	-6.2	-1.94	4.26	6.2	1.94	-4.08	2.11	4.07	3.89
7c	-5.62	-2.48	3.14	5.62	2.48	-4.05	1.57	4.05	5.23
7f	-6.29	-2.06	4.23	6.29	2.06	-4.18	2.12	4.18	4.12
7l	-6.32	-2.17	4.16	6.32	2.16	-4.24	2.08	4.24	4.33

3.5.3. Molecular Electrostatic Maps

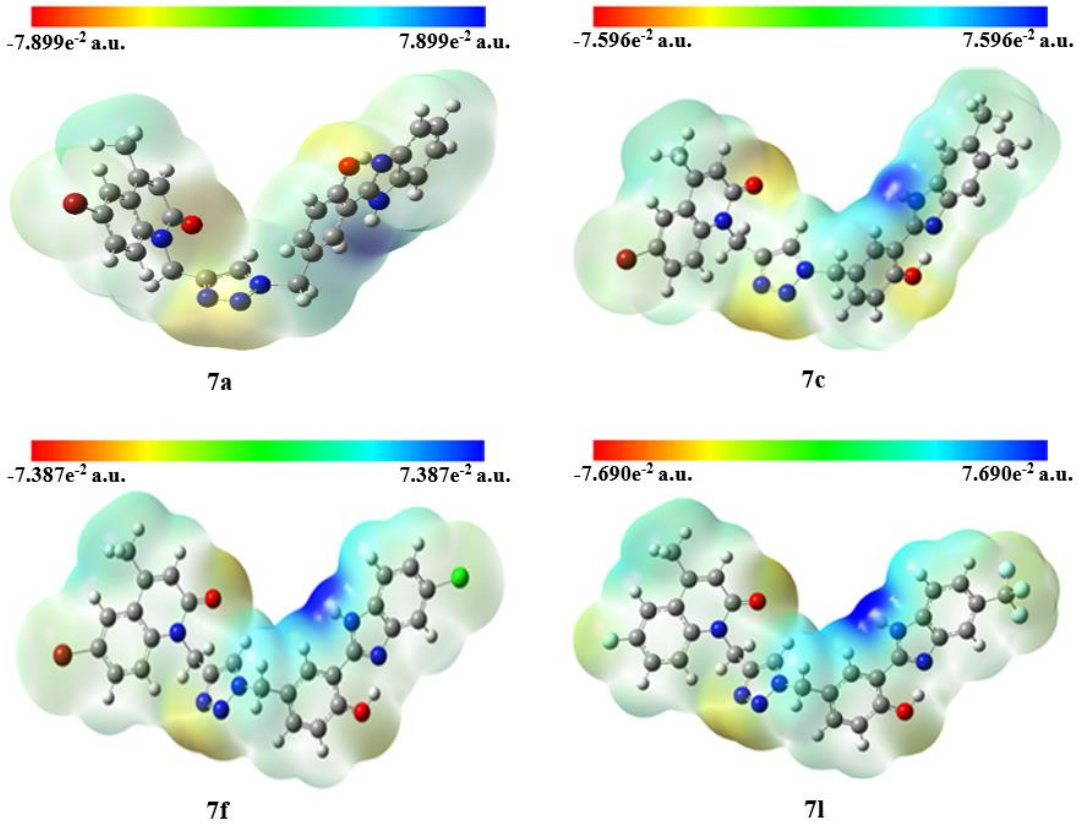

Fig. 7. MEP diagrams of compounds **7a**, **7c**, **7f** and **7l** at B3LYP/6-31+G(d,p) level.

The molecular electrostatic potential (MEP) of the synthesized hybrids **7a**, **7c**, **7f** and **7l** was also evaluated to predict the reactive sites that facilitate interaction within the receptor protein. Indeed, the MEP gives information about the charge distribution of these molecules and their behavior towards electrophilic and nucleophilic attacks. The MEP maps of the four compounds are shown in Fig. 7. The red color refers to the highly negative charged region, whereas the blue region is positively charged.

The negative charge is mainly situated on the nitrogen atoms of the triazole ring along with the carbonyl and the hydroxyl groups, which represent possible sites of electrophilic attack. Notably, the strongest positive potential is at the hydrogen atom bonded to the nitrogen atom of the benzimidazole ring. The remaining zones are also positively polarized and thereby constitute nucleophilic sites, which may render the investigated molecules prone to generating intermolecular hydrogen bonds.

3.6. Molecular docking

As already mentioned in this paper, DNA gyrase is a potential therapeutic target for the identification and development of antibacterial agents. It is composed of two subunits DNA gyrase A (GyrA) and DNA gyrase B (GyrB). The Gyr A subunit is responsible for the breakage and reunion of the double DNA strand, while the GyrB subunit contains the ATPase domain [59]. Quinolones [60] as well as several benzimidazole [61] and 1,2,3-triazole [62] derivatives have been reported to inhibit DNA gyrase. Therefore, compounds **7f** and **7l** having good inhibition potential against *S. aureus* were subjected to molecular docking analysis in an attempt to explore their mode of action against GyrA and GyrB of *S. aureus*.

First, the docking protocol was validated by re-docking the cognate ligands into the active site of the corresponding protein. The re-docked and crystal conformations of the native ligands were well aligned with RMSD less than 1 Å, indicating the validity of the applied protocol (See Fig. S75 and S76 in the supplementary data). The results of the binding affinity of the investigated molecules and their interactions with amino acid residues of target proteins are detailed in Table 7. The best docked poses of the ligands and their 2D interactions are presented in Fig. 8 and 9. The docking experiments with the 2XCT protein (GyrA) revealed that hybrids **7f** and **7l** could fit into the binding pocket with good docking scores of -11.3 and -11.5 kcal/mol, respectively, with reference to ampicillin (-7.2 kcal/mol). Remarkably, **7f** made four hydrogen bonds with the following amino acid residues ARG458, DG9 and DG8, whereas **7l** formed seven hydrogen bonds with ARG1122, ARG458, DG9 and GLY1082. Concerning the 3G75 protein (GyrB), compounds **7f** and **7l** had energy scores of -8.7 and -8.2 kcal/mol, respectively, while ampicillin exhibited a docking score of -6.2 kcal/mol. At the binding site of GyrB, **7f** created three hydrogen bonds with GLU58 and ASN54. Likewise, **7l** interacted *via* three hydrogen bonds to SER55, GLU58 and PRO87 amino acids of 3G75. The main functional groups involved in hydrogen bonding interactions were the oxygen atom of the carbonyl group of the quinolone moiety and the nitrogen atoms of the triazole scaffold. The NH of the imidazole unit and the OH of the phenolic ring acted as hydrogen bond donors. Meanwhile, the chlorine atom in **7f** and the fluorine atoms in **7l** served as hydrogen bond acceptors. Other types of contacts (i.e. Pi-anion, Pi-sigma, Pi-Pi stacked, Pi-alkyl, alkyl-alkyl and halogen (fluorine)) with different amino acid

residues were also observed in both proteins. These findings are in correlation with the DFT predictions.

All in all, compounds **7f** and **7l** had better docking scores and formed more interactions (hydrogen bonds and hydrophobic interactions) than the standard ampicillin, which was in line with the *in vitro* experiments. More also, it was noticed that the docked compounds have more affinity for GyrA than for GyrB and thus they probably show their antibacterial activity against *S. aureus* by inhibiting DNA gyrase A. Lastly, it is worth mentioning that the docking study highlighted the important role of each pharmacophore of hybrids **7f** and **7l** in the binding mechanism.

Table 7

Docking scores (in kcal/mol) and interactions of ampicillin and compounds **7f** and **7l** with amino acid residues of target proteins in *S. aureus*

Compound	Docking score (kcal/mol)	H-bonds interactions	Residual interactions
		GyrA (PDB: 2xct)	
7f	-11.3	ARG458 (2)[a], DG9, DG8	DG8, DC12, DC13, DG9, ARG458
7l	-11.5	ARG1122, ARG458 (3) [a], DG9, GLY1082 (2) [a]	ARG1122, DG8 (5)[b], DC12, DC13, DG9 (5) [b], ARG458
Ampicillin	-7.2	DG9, DC13, DT10 (2) [a]	DC13, DG9 (2) [b]
		GyrB (PDB: 3g75)	
7f	-8.7	GLU58, ASN54 (2) [a]	ASP57, GLU58, ILE86 (3)[b], ILE102 (2) [b]
7l	-8.2	SER55, GLU58, PRO87	ASP81 (2) [b], GLU58, ILE102 (3) [b], ILE86 (3) [b]
Ampicillin	-6.2	ILE102	VAL131

[a] Number of hydrogen bonds

[b] Number of interactions made with binding site residues

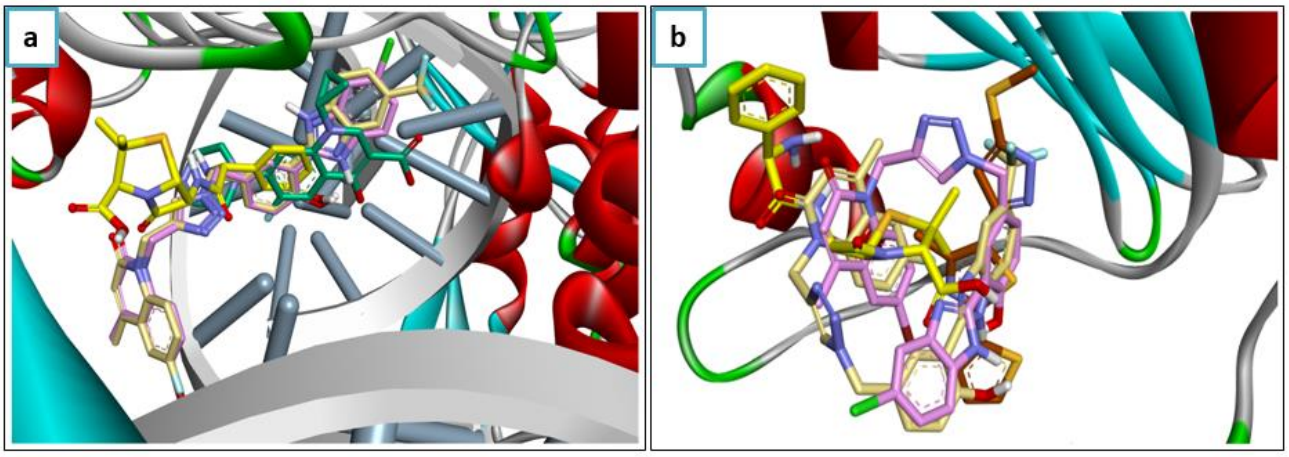

Fig. 8. Conformations of docked molecules **7f** (lavender rose), **7l** (drover) and ampicillin (yellow) along with co-crystallized ligands: a) ciprofloxacin (Persian green) in *S. aureus* DNA gyrase A and b) 4-methyl-5-[3-(methylsulfanyl)-1*H*-pyrazol-5-yl]-2-thiophen-2-yl-1,3-thiazole (rust) in *S. aureus* DNA gyrase B.

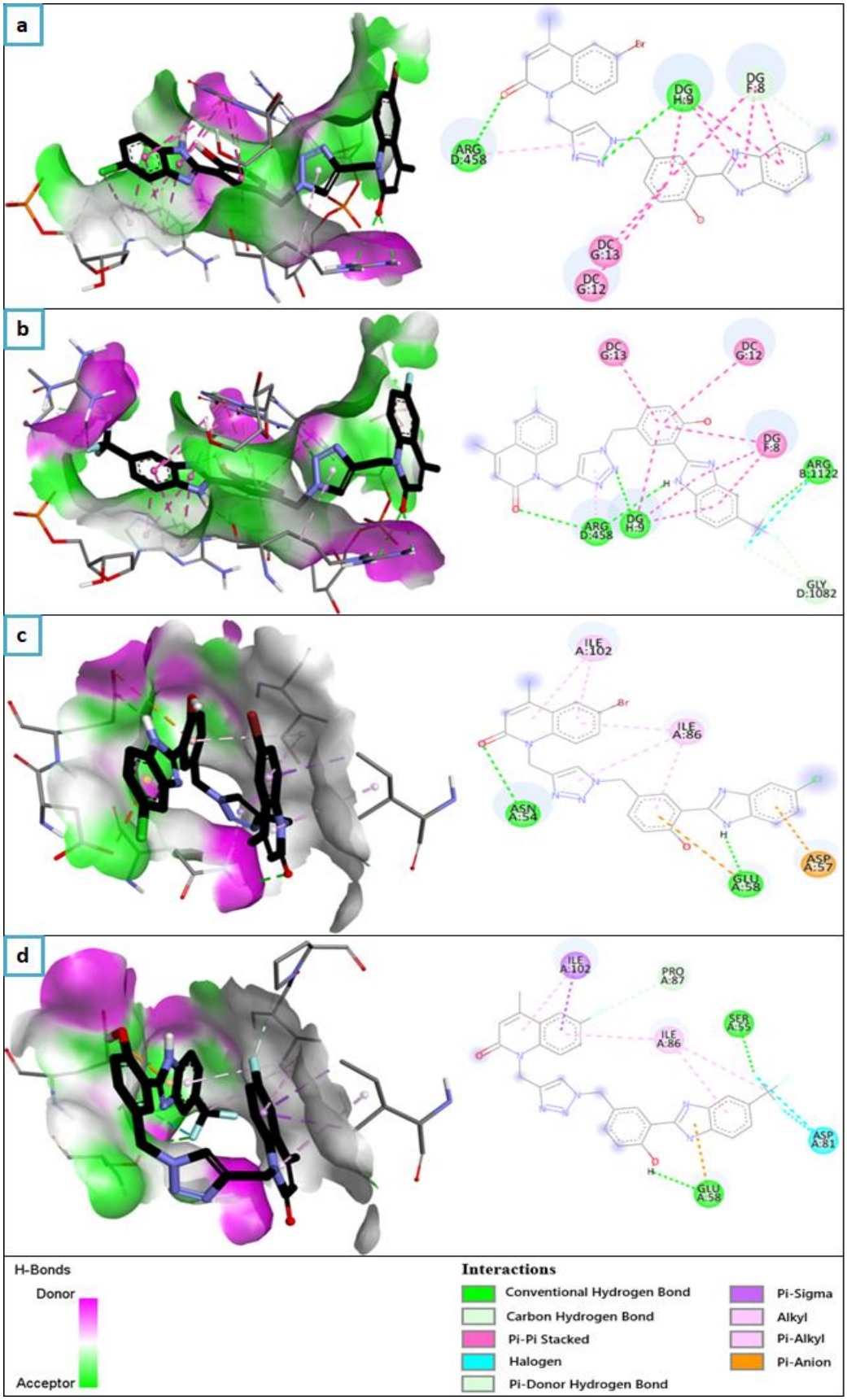

Fig. 9. 2D and 3D representations of binding interactions of docked compounds within active sites of the proteins: a) **7f**-GyrA, b) **7l**-GyrA, c) **7f**-GyrB and d) **7l**-GyrB.

4. Conclusion

In summary, a series of novel compounds containing 2-quinolone, 1,2,3-triazole and benzimidazole moieties in one scaffold were successfully synthesized and characterized by spectral analysis. The structures of compounds **6b** and **7a** were additionally verified by single crystal X-ray diffraction. Antibacterial screening showed that compounds **7a**, **7c**, **7f** and **7l** exhibited similar MIC values against *E. coli* and are nearly twice as potent as the reference drug ampicillin. In case of *S. aureus*, compounds **7f** and **7l** displayed appreciable inhibitory activity with MIC values almost 4 and 2 times less than that of ampicillin, respectively. Moreover, the MBC/MIC ratios demonstrated that all the tested compounds are bactericidal not just bacteriostatic. In addition, the optimized molecular structures, reactivity, stability and quantum chemical parameters of compounds **7a**, **7c**, **7f** and **7l** were investigated using DFT calculations. In general, it was found that the open conformation of these molecules could interact with the biological receptor by the formation of hydrogen bonds or other non-covalent interactions. Finally, the docking analysis against DNA gyrase A and DNA gyrase B of *S. aureus* indicated that DNA gyrase A inhibition is likely responsible for the antibacterial activity of compounds **7f** and **7l**.

ORCID:

Hassan B. Lazrek orcid:0000-0002-3849-9092. Arie.Van-der-lee orcid: 0000-0002-4567-1831.

Ahmad.Mehdi orcid: 0000-0002-7830-2012.

Declaration of Competing Interest

The authors declare that they have no known competing financial interests or personal relationships that could have appeared to influence the work reported in this paper.

Acknowledgement

The authors would like to thank the technical staff of the CAC (Centre of Analysis and Characterization), University Cadi Ayyad for running the spectroscopic analysis,

CRediT authorship contribution statement

Khadija Elgadali: Methodology, Writing – original draft, Software, Data curation. **Meriem Rafya:** Methodology, Writing – original draft, Data curation. **Az-eddine El Mansouri:** Data curation, Formal analysis, Software, Methodology. **Ahmad Mehdi:** Methodology, Writing – review & editing. **Mohamed Maatallah:** Methodology, Writing – review & editing. **Arie Van-der-lee:** Methodology, Writing – review & editing**. Abdelaaziz Ouahrouch:** Formal analysis, Supervision and Methodology. **Fatiha Benkhalti:** Formal analysis, Supervision and Methodology. **Yogesh sanghvi:** Validation, Supervision, Writing – review & editing. **Moha Taourirte:** Data curation, Formal analysis, Methodology, Supervision, Writing – review & editing **H.B.Lazrek:** Conceptualization, Methodology, Project administration,Validation, Supervision, Writing – review & editing.

References

[1] J. Murugaiyan, P.A. Kumar, G.S. Rao, K. Iskandar, S. Hawser, J.P. Hays, Y. Mohsen, S. Adukkadukkam, W.A. Awuah, R.A.M. Jose, N. Sylvia, E.P. Nansubuga, B. Tilocca, P. Roncada, N. Roson-Calero, J. Moreno-Morales, R. Amin, B.K. Kumar, A. Kumar, A.-R. Toufik, T.N. Zaw, O.O. Akinwotu, M.P. Satyaseela, M.B.M. van Dongen, Progress in Alternative Strategies to Combat Antimicrobial Resistance: Focus on Antibiotics, Antibiotics. 11 (2022). https://doi.org/10.3390/antibiotics11020200.

[2] Y. Guo, G. Song, M. Sun, J. Wang, Y. Wang, Prevalence and Therapies of Antibiotic-Resistance in Staphylococcus aureus, Front. Cell. Infect. Microbiol. 10 (2020) 107. https://doi.org/10.3389/fcimb.2020.00107.

[3] S. Deinhardt-Emmer, K. Rennert, E. Schicke, Z. Cseresnyés, M. Windolph, S. Nietzsche, R. Heller, F. Siwczak, K.F. Haupt, S. Carlstedt, M. Schacke, M.T. Figge, C. Ehrhardt, B. Löffler, A.S. Mosig, Co-infection with Staphylococcus aureus after primary influenza virus infection leads to damage of the endothelium in a human alveolus-on-a-chip model, Biofabrication. 12 (2020) 025012. https://doi.org/10.1088/1758-5090/ab7073.

[4] J.R. Adalbert, K. Varshney, R. Tobin, R. Pajaro, Clinical outcomes in patients co-infected with COVID-19 and Staphylococcus aureus: a scoping review, BMC Infectious Diseases. 21 (2021) 985. https://doi.org/10.1186/s12879-021-06616-4.

[5] S.O. Simonetti, E.L. Larghi, T.S. Kaufman, The 3,4-dioxygenated 5-hydroxy-4-aryl-quinolin-2(1H)-one alkaloids. Results of 20 years of research, uncovering a new family of natural products, Nat. Prod. Rep. 33 (2016) 1425–1446. https://doi.org/10.1039/C6NP00064A.

[6] X.-F. Mou, X. Liu, R.-F. Xu, M.-Y. Wei, Y.-W. Fang, C.-L. Shao, Scopuquinolone B, a new monoterpenoid dihydroquinolin-2(1 *H*)-one isolated from the coral-derived *Scopulariopsis* sp. fungus, Natural Product Research. 32 (2018) 773–776. https://doi.org/10.1080/14786419.2017.1359177.

[7] M.A. Eshonov, Kh.A. Rasulova, Acutinine – A New Quinolin-2-One Alkaloid from Haplophyllum acutifolium, Chem Nat Compd. 56 (2020) 509–510. https://doi.org/10.1007/s10600-020-03073-4.

[8] Y.-H. Li, X. Liu, M. Yin, F. Liu, B. Wang, X. Feng, Q.-Z. Wang, Two new quinolone alkaloids from the nearly ripe fruits of *Tetradium ruticarpum*, Natural Product Research. 34 (2020) 1868–1873. https://doi.org/10.1080/14786419.2019.1566819.

[9] O. Moussaoui, R. Bhadane, R. Sghyar, J. Ilaš, E.M. El Hadrami, S. Chakroune, O.M.H. Salo-Ahen, Design, Synthesis, in vitro and in silico Characterization of 2-Quinolone-L-alaninate-1,2,3-triazoles as Antimicrobial Agents, ChemMedChem. 17 (2022) e202100714. https://doi.org/10.1002/cmdc.202100714.

[10] E. Moynihan, K. Mackey, M.A.T. Blaskovich, F.J. Reen, G. McGlacken, N-Alkyl-2-Quinolonopyrones Demonstrate Antimicrobial Activity against ESKAPE Pathogens Including Staphylococcus aureus, ACS Med Chem Lett. 13 (2022) 1358–1362. https://doi.org/10.1021/acsmedchemlett.2c00185.

[11] P. Kaur, Anuradha, A. Chandra, T. Tanwar, S.K. Sahu, A. Mittal, Emerging quinoline- and quinolone-based antibiotics in the light of epidemics, Chemical Biology & Drug Design. 100 (2022) 765–785. https://doi.org/10.1111/cbdd.14025.

[12] M. Durcik, T. Tomašič, N. Zidar, A. Zega, D. Kikelj, L.P. Mašič, J. Ilaš, ATP-competitive DNA gyrase and topoisomerase IV inhibitors as antibacterial agents, Expert Opinion on Therapeutic Patents. 29 (2019) 171–180. https://doi.org/10.1080/13543776.2019.1575362.

[13] S.N. Dighe, T.A. Collet, Recent advances in DNA gyrase-targeted antimicrobial agents, European Journal of Medicinal Chemistry. 199 (2020) 112326. https://doi.org/10.1016/j.ejmech.2020.112326.

[14] Y.A. Ammar, A.A. Farag, A.M. Ali, A. Ragab, A.A. Askar, D.M. Elsisi, A. Belal, Design, synthesis, antimicrobial activity and molecular docking studies of some novel di-substituted sulfonylquinoxaline derivatives, Bioorganic Chemistry. 104 (2020) 104164. https://doi.org/10.1016/j.bioorg.2020.104164.

[15] A.Y. Alzahrani, Y.A. Ammar, M.A. Salem, M. Abu-Elghait, A. Ragab, Design, synthesis, molecular modeling, and antimicrobial potential of novel 3-[(1H-pyrazol-3-yl)imino]indolin-2-one derivatives as DNA gyrase inhibitors, Archiv Der Pharmazie. 355 (2022) 2100266. https://doi.org/10.1002/ardp.202100266.

[16] A.Y. Alzahrani, Y.A. Ammar, M. Abu-Elghait, M.A. Salem, M.A. Assiri, T.E. Ali, A. Ragab, Development of novel indolin-2-one derivative incorporating thiazole moiety as DHFR and quorum sensing inhibitors: Synthesis, antimicrobial, and antibiofilm activities with molecular modelling study, Bioorganic Chemistry. 119 (2022) 105571. https://doi.org/10.1016/j.bioorg.2021.105571.

[17] A.K. Singh, A. Kumar, H. Singh, P. Sonawane, H. Paliwal, S. Thareja, P. Pathak, M. Grishina, M. Jaremko, A.-H. Emwas, J.P. Yadav, A. Verma, H. Khalilullah, P. Kumar, Concept of Hybrid Drugs and Recent Advancements in Anticancer Hybrids, Pharmaceuticals. 15 (2022). https://doi.org/10.3390/ph15091071.
[18] A. Rani, G. Singh, A. Singh, U. Maqbool, G. Kaur, J. Singh, CuAAC-ensembled 1,2,3-triazole-linked isosteres as pharmacophores in drug discovery: review, RSC Advances. 10 (2020) 5610–5635. https://doi.org/10.1039/C9RA09510A.
[19] B. Zhang, Comprehensive review on the anti-bacterial activity of 1,2,3-triazole hybrids, European Journal of Medicinal Chemistry. 168 (2019) 357–372. https://doi.org/10.1016/j.ejmech.2019.02.055.
[20] P. Shiri, A.M. Amani, T. Mayer-Gall, A recent overview on the synthesis of 1,4,5-trisubstituted 1,2,3-triazoles, Beilstein Journal of Organic Chemistry. 17 (2021) 1600–1628. https://doi.org/10.3762/bjoc.17.114.
[21] H. Kaoukabi, Y. Kabri, C. Curti, M. Taourirte, J.C. Rodriguez-Ubis, R. Snoeck, G. Andrei, P. Vanelle, H.B. Lazrek, Dihydropyrimidinone/1,2,3-triazole hybrid molecules: Synthesis and anti-varicella-zoster virus (VZV) evaluation, European Journal of Medicinal Chemistry. 155 (2018) 772–781. https://doi.org/10.1016/j.ejmech.2018.06.028.
[22] M.M. Alam, 1,2,3-Triazole hybrids as anticancer agents: A review, Arch Pharm (Weinheim). 355 (2022) e2100158. https://doi.org/10.1002/ardp.202100158.
[23] S. Sood, R. Bala, V. Kumar, N. Singh, K. Singh, Iodine Mediated Synthesis of Thiabendazole Derivatives and Their Antimicrobial Evaluation, CBC. 14 (2018) 273–277. https://doi.org/10.2174/1573407213666170407160418.
[24] Henriquez-Camacho C, Gotuzzo, E, Echevarria, J, White Jr, AC, Terashima, A, Samalvides, F, Pérez-Molina, JA, M. Plana, Ivermectin versus albendazole or thiabendazole for Strongyloides stercoralis infection, Cochrane Database of Systematic Reviews. (2016). https://doi.org/10.1002/14651858.CD007745.pub3.
[25] Y.T. Lee, Y.J. Tan, C.E. Oon, Benzimidazole and its derivatives as cancer therapeutics: The potential role from traditional to precision medicine, Acta Pharmaceutica Sinica B. (2022). https://doi.org/10.1016/j.apsb.2022.09.010.
[26] H.P. Parkman, Chapter 24 - Prokinetic agents for gastroparesis, in: R.W. McCallum, H.P. Parkman (Eds.), Gastroparesis, Academic Press, 2021: pp. 323–339. https://doi.org/10.1016/B978-0-12-818586-5.00024-7.
[27] A. González-Rodríguez, J.A. Monreal, M. Natividad, M.V. Seeman, Seventy Years of Treating Delusional Disorder with Antipsychotics: A Historical Perspective, Biomedicines. 10 (2022). https://doi.org/10.3390/biomedicines10123281.
[28] A. Malakar, M. Kumar, A. Reddy, H.T. Biswal, B.B. Mandal, G. Krishnamoorthy, Aggregation induced enhanced emission of 2-(2′-hydroxyphenyl)benzimidazole, Photochem. Photobiol. Sci. 15 (2016) 937–948. https://doi.org/10.1039/C6PP00122J.
[29] Y.S. El-Sayed, M. Gaber, M.N. El-Nahass, Structural elucidation, spectroscopic, and metallochromic studies of 2-(2-hydroxy phenyl)-1-H–benzimidazole complexes: Metal ions sensing, DNA binding, and antimicrobial activity evaluation, Journal of Molecular Structure. 1229 (2021) 129809. https://doi.org/10.1016/j.molstruc.2020.129809.
[30] A. Aragón-Muriel, Y. Liscano-Martínez, E. Rufino-Felipe, D. Morales-Morales, J. Oñate-Garzón, D. Polo-Cerón, Synthesis, biological evaluation and model membrane studies on metal complexes containing aromatic N,O-chelate ligands, Heliyon. 6 (2020) e04126. https://doi.org/10.1016/j.heliyon.2020.e04126.
[31] E. Alterhoni, A. Tavman, M. Hacioglu, O. Şahin, A. Seher Birteksöz Tan, Synthesis, structural characterization and antimicrobial activity of Schiff bases and benzimidazole derivatives and their complexes with CoCl2, PdCl2, CuCl2 and ZnCl2, Journal of Molecular Structure. 1229 (2021) 129498. https://doi.org/10.1016/j.molstruc.2020.129498.
[32] A.M.Y. Moustafa, S.B. Bakare, Synthesis of Some Hybrid 7-Hydroxy Quinolinone Derivatives As Anti Breast Cancer Drugs, Res Chem Intermed. 45 (2019) 3895–3912. https://doi.org/10.1007/s11164-019-03827-y.
[33] M.J. Ahsan, R.K. Kumawat, S.S. Jadav, M.H. Geesi, M.A. Bakht, M. Hassan, A. Al-Tamimi, Y. Riadi, A. Hussain, N.M. Ganta, Synthesis, cytotoxic evaluation, and molecular docking studies of N-(7-hydroxy-4-methyl-2-oxoquinolin-1 (2H)-yl) acetamide/benzamide analogues, Letters in Drug Design & Discovery. 16 (2019) 182–193.

[34] A.R. Han, E.H. Jeon, K.W. Kim, S.K. Lee, C. Ohn, S.J. Park, N.S. Kang, T.-S. Koo, K.B. Hong, S. Choi, Synthesis and biological evaluation of quinolone derivatives as transthyretin amyloidogenesis inhibitors and fluorescence sensors, Bioorganic & Medicinal Chemistry. 53 (2022) 116550. https://doi.org/10.1016/j.bmc.2021.116550.
[35] A.D. Cort, L. Mandolini, C. Pasquini, L. Schiaffino, A novel ditopic zinc-salophen macrocycle: a potential two-stationed wheel for [2]-pseudorotaxanes, Org. Biomol. Chem. 4 (2006) 4543. https://doi.org/10.1039/b613705a.
[36] W. Si, T. Zhang, Y. Li, D. She, W. Pan, Z. Gao, J. Ning, X. Mei, Synthesis and biological activity of novel benzimidazole derivatives as potential antifungal agents, Journal of Pesticide Science. 41 (2015) 15–19. https://doi.org/10.1584/jpestics.D15-037.
[37] A.X.S. Bruker, APEX3 Package, APEX3, SAINT and SADABS, (2016).
[38] A. van der Lee, Charge flipping for routine structure solution, J Appl Crystallogr. 46 (2013) 1306–1315. https://doi.org/10.1107/S0021889813020049.
[39] L. Palatinus, G. Chapuis, *SUPERFLIP* – a computer program for the solution of crystal structures by charge flipping in arbitrary dimensions, J Appl Crystallogr. 40 (2007) 786–790. https://doi.org/10.1107/S0021889807029238.
[40] P.W. Betteridge, J.R. Carruthers, R.I. Cooper, K. Prout, D.J. Watkin, Crystals suite of programs, J. Appl. Crystallogr. 36 (2003) 1487.
[41] R.I. Cooper, A.L. Thompson, D.J. Watkin, *CRYSTALS* enhancements: dealing with hydrogen atoms in refinement, J Appl Crystallogr. 43 (2010) 1100–1107. https://doi.org/10.1107/S0021889810025598.
[42] P.A. Wayne, Clinical and laboratory standards institute. Performance standards for antimicrobial susceptibility testing, (2011).
[43] M. Frisch, G.W. Trucks, H.B. Schlegel, G.E. Scuseria, M.A. Robb, J.R. Cheeseman, G. Scalmani, V. Barone, B. Mennucci, Ga. Petersson, Gaussian 09, revision D. 01, (2009).
[44] A. Frisch, A.B. Nielson, A.J. Holder, Gaussview user manual, Gaussian Inc., Pittsburgh, PA. 556 (2000).
[45] C. Lee, W. Yang, R.G. Parr, Development of the Colle-Salvetti correlation-energy formula into a functional of the electron density, Physical Review B. 37 (1988) 785.
[46] B. Miehlich, A. Savin, H. Stoll, H. Preuss, Results obtained with the correlation energy density functionals of Becke and Lee, Yang and Parr, Chemical Physics Letters. 157 (1989) 200–206.
[47] T. Koopmans, Über die Zuordnung von Wellenfunktionen und Eigenwerten zu den einzelnen Elektronen eines Atoms, Physica. 1 (1934) 104–113.
[48] O. Trott, A.J. Olson, AutoDock Vina: Improving the speed and accuracy of docking with a new scoring function, efficient optimization, and multithreading, J. Comput. Chem. (2009) NA-NA. https://doi.org/10.1002/jcc.21334.
[49] L. Knorr, Synthetic Experiments with Acetoacetic Ester, Justus Liebigs Ann Chem. 236 (1886) 69–115.
[50] N. Wlodarczyk, C. Simenel, M. Delepierre, J.-C. Barale, Y. Janin, On the Knorr Synthesis of 6-Bromo-4-methylquinolin-2(1H)-one, Synthesis. 2011 (2011) 934–942. https://doi.org/10.1055/s-0030-1258440.
[51] L. E, RestrepoJelem, PerezBianca, OrtizShelby, SalazarJose, One Pot Microwave Promoted Synthesis of 2-Aryl-1H-Benzimidazoles Using Sodium Hydrogen Sulfite, Bulletin of the Korean Chemical Society. 30 (2009) 1628–1630.
[52] W.D. Guerra, E. Odella, M. Secor, J.J. Goings, M.N. Urrutia, B.L. Wadsworth, M. Gervaldo, L.E. Sereno, T.A. Moore, G.F. Moore, S. Hammes-Schiffer, A.L. Moore, Role of Intact Hydrogen-Bond Networks in Multiproton-Coupled Electron Transfer, J. Am. Chem. Soc. 142 (2020) 21842–21851. https://doi.org/10.1021/jacs.0c10474.
[53] I.J. Bruno, J.C. Cole, M. Kessler, J. Luo, W.D.S. Motherwell, L.H. Purkis, B.R. Smith, R. Taylor, R.I. Cooper, S.E. Harris, A.G. Orpen, Retrieval of Crystallographically-Derived Molecular Geometry Information, J. Chem. Inf. Comput. Sci. 44 (2004) 2133–2144. https://doi.org/10.1021/ci049780b.
[54] S.J. Cottrell, T.S.G. Olsson, R. Taylor, J.C. Cole, J.W. Liebeschuetz, Validating and Understanding Ring Conformations Using Small Molecule Crystallographic Data, J. Chem. Inf. Model. 52 (2012) 956–962. https://doi.org/10.1021/ci200439d.
[55] C.R. Groom, I.J. Bruno, M.P. Lightfoot, S.C. Ward, The Cambridge Structural Database, Acta Crystallogr B Struct Sci Cryst Eng Mater. 72 (2016) 171–179. https://doi.org/10.1107/S2052520616003954.
[56] C.F. Macrae, I. Sovago, S.J. Cottrell, P.T.A. Galek, P. McCabe, E. Pidcock, M. Platings, G.P. Shields, J.S. Stevens, M. Towler, P.A. Wood, *Mercury 4.0* : from visualization to analysis, design and prediction, J Appl Crystallogr. 53 (2020) 226–235. https://doi.org/10.1107/S1600576719014092.

[57] P.T.A. Galek, L. Fábián, W.D.S. Motherwell, F.H. Allen, N. Feeder, Knowledge-based model of hydrogen-bonding propensity in organic crystals, Acta Crystallogr B Struct Sci. 63 (2007) 768–782. https://doi.org/10.1107/S0108768107030996.
[58] R. Mogana, A. Adhikari, M.N. Tzar, R. Ramliza, C. Wiart, Antibacterial activities of the extracts, fractions and isolated compounds from Canarium patentinervium Miq. against bacterial clinical isolates, BMC Complementary Medicine and Therapies. 20 (2020) 55. https://doi.org/10.1186/s12906-020-2837-5.
[59] A. Maxwell, D.M. Lawson, The ATP-binding site of type II topoisomerases as a target for antibacterial drugs, Current Topics in Medicinal Chemistry. 3 (2003) 283–303.
[60] S. Jaswal, B. Nehra, S. Kumar, V. Monga, Recent advancements in the medicinal chemistry of bacterial type II topoisomerase inhibitors, Bioorganic Chemistry. 104 (2020) 104266. https://doi.org/10.1016/j.bioorg.2020.104266.
[61] M. Gjorgjieva, T. Tomašič, M. Barančokova, S. Katsamakas, J. Ilaš, P. Tammela, L. Peterlin Mašič, D. Kikelj, Discovery of Benzothiazole Scaffold-Based DNA Gyrase B Inhibitors, J. Med. Chem. 59 (2016) 8941–8954. https://doi.org/10.1021/acs.jmedchem.6b00864.
[62] K. Lal, P. Yadav, A. Kumar, A. Kumar, A.K. Paul, Design, synthesis, characterization, antimicrobial evaluation and molecular modeling studies of some dehydroacetic acid-chalcone-1,2,3-triazole hybrids, Bioorganic Chemistry. 77 (2018) 236–244. https://doi.org/10.1016/j.bioorg.2018.01.016.

Captions of schemes and figures

Scheme 1. Synthesis of starting compounds.

Scheme 2. Synthesis of novel hybrid compounds based on quinolin-2-one.

Figure 1. Examples of antimicrobial agents and design strategy of target structures.

Figure 2. ORTEP style drawings of the molecular structures of **6b** and **7a** based on the results from the X-ray diffraction analyses. The anisotropic atomic displacement ellipsoids have been drawn at the 50% probability level.

Figure 3. Comparison of MICs (μmol/mL) of tested compounds (**6a,b** and **7a-n)** and ampicillin (Amp).

Figure 4. DFT-optimized structures of conformers (A) of **7a**, **7c**, **7f** and **7l** in the gas phase.

Figure 5. DFT-optimized structures of conformers (B) of **7a**, **7c**, **7f** and **7l** in the gas phase.

Figure 6. HOMO-LUMO of **7a**, **7c**, **7f**, and **7l** compounds at B3LYP/6-31+G(d,p) level.

Figure 7. MEP diagrams of compounds **7a**, **7c**, **7f** and **7l** at B3LYP/6-31+G(d,p) level.

Figure 8. Conformations of docked molecules **7f** (lavender rose), **7l** (drover) and ampicillin (yellow) along with co-crystallized ligands: a) ciprofloxacin (Persian green) in *S. aureus* DNA gyrase A and b) 4-methyl-5-[3-(methylsulfanyl)-1*H*-pyrazol-5-yl]-2-thiophen-2-yl-1,3-thiazole (rust) in *S. aureus* DNA gyrase B.

Figure 9. 2D and 3D representations of binding interactions of docked compounds within active sites of the proteins: a) **7f**-GyrA, b) **7l**-GyrA, c) **7f**-GyrB and d) **7l**-GyrB.